THE COHERENT STRUCTURE OF TURBULENT MIXING LAYERS

I. SIMILARITY OF THE PRIMARY VORTEX STRUCTURE

II. SECONDARY STREAMWISE VORTEX STRUCTURE

Thesis by

Luis P. Bernal

In Partial Fulfillment of the Requirements

for the Degree of

Doctor of Philosophy

California Institute of Technology

Pasadena, California

1981

(Submitted May 19, 1981)

Acknowledgements

This work would not have been completed without the continuous support and encouragement of Professor Anatol Roshko. His suggestions have motivated every aspect of this research. His guidance was instrumental in its development. Numerous discussions provided valuable insight in the results. His assistance is deeply appreciated.

I have benefited from numerous suggestions and discussions with Drs. D. Coles, P. E. Dimotakis, J. E. Broadwell, R. E. Breidenthal and G. L. Brown. I would also like to express my appreciation to the members of my Thesis committee, Dr. H. Nagib and Mr. R. Roberts for their comments on the content of this Thesis.

To Earl Dahl who helped with the experiments, Harry Hamaguchi who assisted with the photography, Kathy Franson who typed the manuscript and Betty Wood who assisted with the figures, my gratitude for their professional competence.

I would like to thank Dr. W. Knauss of GALCIT's Solid Mechanics group and Drs. T. Wu and G. Yates of Engineering Science for the use of their photographic equipment, Dr. J. Bonner of Biology and Dr. J. M. Sala-Trepat for the use of the digitizer and Mr. P. Massier and Dr. V. Sarohia of the Jet Propulsion Laboratory for the use of a strobe light source.

The research was supported by the Department of the Navy, by the Office of Naval Research, under Contracts Nos. 8960-1 and N00014-79-C-0365 from Project SQUID and Contract No. N00014-76-C-0260 from the Fluid Dynamics Program.

To the members of the GALCIT faculty, students, technical staff and their spouses my gratitude. Their friendship will always be remembered.

Finally to my wife Sara, children Luis-Manuel and Sara, to my Parents and Parents-in-law my deepest appreciation for your support, encouragement and endurance during these years.

Abstract

The primary spanwise organized vortex structure and the secondary streamwise vortex structure of turbulent mixing layers have been investigated. Flow visualization motion pictures of a constant density mixing layer were used to measure the properties of the large scale vortices. It was found that after an initial transition region mean properties of the large scale vortices reach the expected linear growth with downstream distance required by similarity. In the self-similar region, the vortex core area and visual thickness increase continuously during its life-span.

A theoretical model of probability distribution function for the large-scale vortex circulation was developed. This distribution is found to be lognormal and to have a standard deviation, normalized with the mean of 0.28. From this model the mean life-span of the vortices could also be obtained and was found to be 0.67 times the mean life-span position.

The streamwise streak pattern observed by Konrad (1976) and Breidenthal (1978) in plan-view pictures of the mixing layer was investigated, using flow visualization and spanwise concentration measurements. It was confirmed that this pattern is the result of a secondary vortex structure dominated by streamwise, counter-rotating vortices. A detailed description of its spatial relation to the primary, spanwise vortex structure is presented. From time average flow pictures, the onset position and initial scale of the secondary structures were determined. From concentration measurements,

spanwise variations in mean properties, resulting from the secondary structure, were found. This also showed an increase of the spanwise scale with downstream distance and the existence of the streamwise vortices in the fully developed turbulent region. In this region the mean spacing is found approximately equal to the vorticity thickness.

Table of Contents

Table of Contents cont'd

List of Symbols

A_c	Primary vortex core area
C	Helium concentration
C_p	Product concentration
C_{A_0}, C_{B_0}	Free stream reactant concentrations
$\tilde{C}_p$	C_p/C_{B_0}
D	Primary vortex core visual thickness
f	C_{A_0}/C_{B_0}
$g(\ell n\ \xi)$	Function defined by Equation I.3.11
$I(\sigma)$	Function defined by Equation I.3.18
k_A, k_F	Number of vortices annihilated/formed per vortex lost by amalgamation
ℓ	Primary vortex circulation
L	Life-span of primary vortices
L_{BL}	Effective length of the boundary-layer on the splitter plate
$n(\ell, x)$	Number of vortices convected through downstream location x with circulation ℓ per unit time
$n_a(\ell, x)$	Change per unit time of the number of vortices of circulation ℓ at x as a result of amalgamations
$n_T(x)$	Total number of vortices convected through x per unit time
$n_A(x)$, $n_F(x)$	Total number of vortices annihilated, formed per unit time at x.

List of Symbols cont'd.

$p(\xi)$, $p_\zeta(\zeta)$	Probability density of vortex circulation and position respectively
$p_A(\xi)$, $p_F(\xi)$	Probability density of vortex annihilation and formation respectively
p_0	Test section static pressure
$q(\xi)$	Overlap function introduced in Equation I.3.16
r	Velocity ratio U_2/U_1
Re_θ	Splitter plate boundary-layer Reynolds number, $U\theta/\nu$
Re_{δ_ω}	Mixing layer Reynolds number $\Delta U\delta_\omega/\nu$
s	Density ratio ρ_2/ρ_2
U	Downstream velocity
U_c	Convection velocity of the primary vortices
x, y, z	Coordinates; x downstream, y across the layer, z along the span
x_0	Virtual origin location
x_t	Downstream extent of the transition region
x_{3D}	Downstream origin of streamwise streaks.
X	Mean life-span position of primary vortices $\frac{\overline{\zeta}_F + \overline{\zeta}_A}{2}$
α	$\ell n\ \xi$
δ_v	Visual thickness
δ_{v_0}	Visual thickness at x_{3D}
δ_ω	Vorticity thickness $\frac{\Delta U}{\left.\frac{\partial u}{\partial y}\right\|_{max}}$

List of Symbols cont'd.

$\delta_{\tilde{C}_p}$	Product thickness $\int_{-\infty}^{\infty} \tilde{C}_p(y)dy$
ΔU	$U_1 - U_2$
$\zeta \equiv \frac{x-x_0}{\ell}$	Similarity variable
$\overline{\zeta}_A$, $\overline{\zeta}_F$	Mean normalized annihilation and formation positions respectively
$\eta \equiv \frac{y}{x-x_0}$	Similarity variable
θ	Splitter plate boundary layer momentum thickness at separation
λ_{3D}	Streamwise streaks spacing at formation
λ_{2Di}	Kelvin-Helmholtz instability wavelength
λ_{2D}	Primary vortex wavelength at x_{3D}
ν	Kinematic viscosity
$\xi = \frac{\ell}{x-x_0}$	Similarity variable
σ	Lognormal distribution parameter describing its width

List of Figures

List of Figures cont'd.

List of Figures cont'd.

Preface

The turbulent mixing layer has been the subject of numerous investigations. Of particular interest are the results of Brown and Roshko (1971, 1974) who discovered the presence at high Reynolds numbers of spanwise organized vortical structures. These vortices are convected downstream during life-times which are terminated when they interact or amalgamate with neighboring vortices to form larger ones. A form of interaction, the pairing interaction, in which two adjacent vortices rotate around each other until they amalgamate, was documented by Winant and Browand (1974) at low and moderate Reynolds numbers. This form of amalgamation and similar ones involving more than two vortices have also been observed by us at high Reynolds numbers (see Roshko, 1976 Dimotakis and Brown 1976 and also Hernan and Jimenez, 1979). The amalgamation of more than two vortices have also been studied in a forced mixing layer by Ho and Huang (1980). Moore and Saffman (1975) suggested a different possible form of amalgamation in which a vortex is torn apart by its neighbors and assimilated into them. Tearing processes were reported by Dimotakis and Brown (1976).

Winant and Browand proposed that the growth of the mixing layer is primarily due to amalgamation processes but Hernan and Jimenez (1979), who processed movies obtained by the present author at much higher Reynolds numbers than those in the experiments of Winant and Browand, found that considerable (possibly primary) growth occurs in individual vortices during their lifetime between coalescences. This observation is consistent with the proposed model of Moore and Saffman in which

continual growth by turbulent entrainment plays an essential role. Their argument is based on the need to ingest irrotational fluid into the vortices so that the necessary decrease in vorticity can occur as the mixing layer grows downstream. At low Reynolds numbers this ingestion could occur by viscous diffusion, as in the flows calculated by Patnaik, Sherman and Corcos (1976), but at high Reynolds numbers it would have to occur by turbulent mixing as suggested by Moore and Saffman.

These views of the primary vortex structure and processes in a mixing layer illustrate the need to consider the effects of what might be called residual turbulence on those processes, i.e., the effects of secondary and possibly high order instabilities (considering the spanwise organized vortices to be the structures resulting from the primary instability).

Pertinent to this discussion is the transition discovered by Konrad (1976) and further explored by Breidenthal (1978), who named it the "mixing transition." The primary, spanwise vortices and their amalgamations exist on both sides of the mixing transition, which is characterized mainly by the appearance, on the high-Reynolds-number side of the transition, of smaller scale, three dimensional structures (as seen on flow visualizations) and by increased "mixedness" (as exhibited by the extent of chemical reaction between reactants carried by the two streams). The development of the smaller scale structure was believed, by Konrad and Breidenthal, to be associated with streamwise

oriented vortex structures whose presence was inferred from the streamwise streaks that were visible on plan views of the mixing layers.

In the present investigations our purpose was to explore further the properties of the primary structures and of the development and effects of secondary, three dimensional structures. The results are presented in two parts.

In Part I, the statistical properties of the primary, spanwise oriented structures are obtained by examining, frame-by-frame, shadowgraph motion pictures of the edge view of mixing layers. A theoretical model of the distribution of vortex strengths, following the lead of Takaki and Kovasznay (1978), is also developed and shown to give a better fit than their model to the experimental data. It also provides insights into the physical processes occurring.

Part II is devoted mainly to an exploration of the effects and nature of the secondary structure associated with the streamwise streaks observed by Konrad and by Breidenthal. In particular, flow visualization in a plane normal to the flow direction confirms their conjecture that the streaks are associated with streamwise vortices. By examination of successive frames in a movie of that plane, a three dimensional, spatial picture of the secondary structure and its relation to the primary structure is constructed. It is consistent with results from concentration measurements that were also made in a mixing layer between streams of helium and nitrogen.

Part I

SIMILARITY OF THE PRIMARY VORTEX STRUCTURE

I.1 Introduction

In this part, we describe our experimental and theoretical studies of the properties of the large vortices in a turbulent mixing layer. It had been found by previous investigators that in a well developed turbulent mixing layer these vortex structures have a broad distribution of sizes at any given downstream position. This distribution is, in a sense, the primary manifestation of the turbulent character of the well developed flow. Another manifestation is the presence of smaller scale, three dimensional structures and motions, but these play only an indirect role in part I. They will be discussed more specifically in part II.

Brown and Roshko (1974) measured the probability distribution of vortex spacing in a mixing layer between helium and nitrogen. Winant and Browand (1974) obtained a similar probability distribution in water at moderate Reynolds number. On the basis of these results Brown and Roshko concluded that the mean spacing normalized with the local vorticity thickness is constant independent of velocity and density ratio, $\overline{\ell} = 3\delta_\omega$. In these investigations self-similarity was shown for the mean velocity and density profiles but was not shown for the mean properties of the vortices. Self-similarity of the vortex spacing is implied by the self-similarity of spectra obtained at various downstream locations (e.g., Kolpin, 1964) and of autocorrelations obtained by Dimotakis and Brown (1976) who found $3.1 < \overline{\ell}/\delta_\omega < 5.0$.

Limited experimental data are available on the evolution of the vortices during their life-times. Brown and Roshko (1974) found the

spacing between vortices to be constant during life-time. On the other hand, the vortex cores, as measured by Hernan and Jimenez (1979) increase in size during their life-times. Furthermore, they found the increase in size of the vortex core during a life-time to be appreciably larger than during amalgamation, i.e., little additional growth of the cores is accomplished by amalgamation.

An aspect of the vortex evolution on which there had been no information so far is the effect of the conditions at formation of a vortex on its subsequent evolution. In the fully developed turbulent region where the vortex cores can be considered turbulent the significant parameters are the characteristic time of the small scale motions within the vortex core and the life-time of the vortex. If the former is much longer the initial conditions will determine the evolution of the vortices. However, if the characteristic time of the small scale motions is much shorter, the vortex evolution can be expected to reach an asymptotic state characterized only by the relevant global parameters, namely its circulation and position.

In this investigation we have used flow visualization motion pictures of a constant density mixing layer to measure the properties of the large scale vortices, to follow their evolution and to characterize their statistical properties.

In addition we have studied the statistical theory of vortex circulation for the self-similar mixing layer. This theory was previously developed by Takaki and Kovasznay (1978) who found reasonable agreement with experimental results. Our formulation is

somewhat different in that, among other things, the results obtained for the probability distribution of vortex circulation are also used to calculate the normalized life span of the vortices.

In this part we first present the experimental results, in Chapter I.2, and then the theoretical discussion, in Chapter I.3, followed by a summary and discussion.

I.2 Flow Visualization Results.

Two different shadowgraph motion pictures of a constant density mixing layer at different Reynolds number have been used to measure the visual properties of the large scale vortices. The experimental technique is described first. The results concerning the vortex circulation (spacing) follow. They were obtained at relatively low Reynolds number, so particular emphasis is made in the distinction between the transition region and the fully developed turbulent region. In the last section the measurements of the visual thickness and core area evolution are presented. These results are compared with several two-dimensional models of the evolution of the large scale vortices. Throughout this presentation reference will be made to the results of the statistical theory presented in the next chapter.

I.2.1 Apparatus and Data Processing

Flow visualization motion pictures were obtained in the gas mixing layer facility described by Brown and Roshko (1974). Nitrogen and a mixture of 33.33% helium in argon were chosen as working fluids because their difference in optical refractive index allows shadowgraph flow visualization of a constant density mixing layer (Konrad, 1976). Two motion pictures were obtained at the same nominal flow velocities of 1000 cm/s and 380 cm/s, but at different static pressures, 4 and 8 atmospheres. A sketch of the mixing layer and coordinate system used is presented in figure I.1. The parameters characterizing the evolution of the layer are the velocity ratio $r = 0.38$ and the

Reynolds number $\Delta U\delta_\omega/\nu_{N_2} = 4.6 \times 10^3$ and 2.5×10^4 for the 4 and 8 atmospheres movies respecitvely. These values of the Reynolds number were calculated using an estimate of the vorticity thickness at x = 8 cm, the test section length used in the experiments.

The shadowgraph optical system is sketched in figure I.2. A mercury arc lamp (.1 mm rectangular light source) is positioned at the focal point of a spherical mirror; the resulting collimated beam, 20 cm in diameter, is sent through the test section in the spanwise direction. The beam is then focused on the film by a 1200 mm f-6.3 lens and a 75 mm camera lens located at the focal point of the preceding lens. A Hycam model K20S4E high speed camera was used at a nominal frame rate of 3000 pictures per second. Actual frame rates were measured using timing marks recorded on the film.

A typical frame from one of the motion pictures is shown in figure I.3. The dark features within it mark regions with large index of refraction gradients on a plane perpendicular to the direction of propagation of the beam, hence such regions mark an interface between fresh fluid form the two streams or between mixed fluid and one of the streams. Adjacent vortices are separated by S shaped lines inclined in the flow direction which are called the "braids" following the terminology of Patnaik et al. (1976). These features are convected by the flow, with some disappearing during the amalgamation process. Pairing (Winant and Browand, 1976) is the most frequent form of amalgamation found in these pictures; it involves the rotation of two

vortices around each other until the intervening braid can no longer be identified.

For the purpose of this investigation a large scale vortex is defined as the region between two successive braid/x-axis intersections irrespective of the braid orientation. For example, the vortices in the left middle of the picture in figure I.3 were considered two different vortices even though the process of pairing may have started already. Whereas the nearly completed pairing in the right middle was considered to be one new vortex. A consequence of this definition is that amalgamation occurs between consecutive frames when a braid disappears.

The large scale vortex properties which were measured are sketched in figure I.4; these are the braid/x-axis intersection, the area A_c and the visual thickness D of the core. The measurements of the braid/x-axis intersections were made with a Kodak film analyser on the film obtained at $p_0 = 4$ atm. This parameter and the area and visual thickness of the core on the film obtained at 8 atm. were measured with a HP 9864 A digitizer (section I.2.3). In both cases reference features (e.g., the channel width) on each frame were utilized to obtain the actual magnifications. The area of the cores was measured with the digitizer by moving the cursor along its periphery. The accuracy of the measurements was limited by the finite thickness of the features that define the large scale vortices on the film itself. They are associated in part with the spanwise nonuniformities described in

part II. Their thickness is approximately constant throughout the length of the layer; when scaled to the experiment size they give a measurement error of 0.3 cm.

The measured locations of adjacent braid/x-axis intersections were used to calculate the distance ℓ between them (figure I.4) and the mid-point between them. The former characterizes not only the spacing of the vortices but also their circulation which is given by the approximate relation

$$\Gamma \doteq \Delta U \cdot \ell$$

For this reason, ℓ is called the circulation of the vortex throughout this work. A constant factor ΔU needs to be applied to obtain its dimensionally correct value. The mid-point between braid/x-axis intersections is defined as the downstream position of the vortex. Good agreement was found between the position of the vortex given by this definition and the downstream location of the center of mass of the core area (2% discrepancy). It should be noted that the parameters measured are geometrical properties of the vortices which are related to changes in the refractive index of the gas mixture and it is not clear how they are related to the vorticity distribution within the vortices.

I.2.2 Vortex Circulation Similarity

The movie obtained at a static pressure of 4 atm., U_1 = 1000 cm/s, r = 0.38, was used to measure the braid/x-axis intersections in a sequence of 600 frames. From these data the position and circulation of the vortices was calculated.

A simple scheme was devised to follow the vortices through several frames. Vortex realizations in two consecutive frames were considered to be the same vortex if their positions in the two frames (x_1, x_2) satisfied the inequality $U_1\tau > x_2 - x_1 > U_2\tau$ where U_1, U_2 are the free stream velocities and τ is the elapsed time between frames. When this technique was applied, a total of 668 vortex time histories were obtained, each one giving the position and circulation of the vortex as a function of time. Each time history was approximated by a straight line in a least squares sense; the rms deviation from the line was found to be always below 1 mm.

Self-similarity was evaluated by considering the properties of the vortices as they were convected across specific downstream positions. Using the time histories, the circulation, its time derivative and the convection velocity of the vortices moving across the eight downstream positions from x = 1 to 8 cm were obtained.

There is some redundancy in the measured data which can be used to evaluate the vortex identification technique. The total length convected through any downstream position is given by $n_T \cdot \bar{\ell}$ where n_T is the total number of vortices and $\bar{\ell}$ the local mean circulation. This quantity is also given by $U_c\tau_s$ where U_c is the measured

convection velocity and τ_s is the duration of the sequence of 600 frames. Therefore

$$n_T = \frac{U_c \tau_s}{\bar{\ell}}$$

This result as well as the actual values of n_T are plotted as a function of $\bar{\ell}$ in figure I.5. The values calculated from the above equation are 12% higher than those obtained by direct counting, indicating that the technique fails to recognize some vortices; the error is independent of downstream position. A second feature shown in this figure is the reduction of the number of vortices with downstream position (increasing $\bar{\ell}$) as the result of amalgamation processes. A loss of 110 vortices, from 165 at $x = 2$ cm to 55 at $x = 8$ cm, occurs in the duration of the sequence.

The downstream evolution of the mean circulation is presented in figure I.6. A linear dependence is found downstream of $x_t = 4$ cm. A least squares fit to the data downstream of this point gives

$$\bar{\ell} = .24\ (x - x_0)$$

with $x_0 = -1.4$ cm. This line is also plotted in the figure. The extent of the transition region and the location of the virtual origin depend on the initial conditions, namely the high speed boundary layer momentum thickness θ_1 and Reynolds number R_{θ_1} (Breidenthal 1978). The boundary layer momentum thickness for the conditions in this experiment, calculated by Thwaites' method, gave

$$\frac{x_t}{\theta_1} = 560, \quad -\frac{x_0}{\theta_1} = 200, \quad R_{\theta_1} = 180$$

These values are compared in table I.1 with the results of Bradshaw (1966) and Hussain and Zedan (1978) in axisymmetric mixing layers and Breidenthal (1978) for a plane layer. The values obtained in this experiment are within the general scatter of those results.

In the self-similar region, the growth rate of mean circulation is $d\bar{\ell}/dx = 0.24$. Using Brown and Roshko's (1974) best-fit line for the growth rate of the vorticity thickness, $d\delta_\omega/dx = 0.081$, gives a relation between $\bar{\ell}$ and δ_ω, that is

$$\frac{\bar{\ell}}{\delta_\omega} = 3.0$$

This value is in excellent agreement with the measurements of Brown and Roshko (1974) for a density ratio of 7 and Winant and Browand (1974) for a constant density mixing layer. A somewhat larger value was measured by Dimotakis and Brown (1976) and by Koochesfahani et al. (1979).

The rms deviation of the circulation normalized with its mean is plotted as a function of downstream distance in figure I.7. A peak is found at $x = 3$ cm in the transition region. Within the self-similar region fluctuations are also encountered. Their amplitude stays within the estimated statistical uncertainty which, as a result of the small sample available, is quite large (10%). The average value of the normalized rms deviation in the self-similar region ($x \geq 4$ cm) is 0.24, slightly lower than the values reported by Brown and Roshko (1974) and Winant and Browand (1974). Koochesfahani et al.(1979) found a much smaller deviation, $\ell'/\bar{\ell} = 0.03$, due perhaps to their vortex identification technique.

In the self-similar region, $x \geq 4$ cm, all vortices in the sample can be used to obtain the normalized circulation probability distribution. A histogram was constructed using $\ell/\overline{\ell}$ as the similarity variable in order to facilitate comparison with other experimental and theoretical results. This histogram is presented in figure I.8. Good agreement is found with the measurements of Brown and Roshko and Winant and Browand. Also plotted in figure I.8 is the theoretical result of Takaki and Kovasznay (1978) and a lognormal distribution with $\ell'/\overline{\ell} = 0.28$, the result of the theory presented in I.3.

The vortex time histories (position x as a function of time and circulation ℓ as function of time) were also used to obtain the convection velocity and rate of change of the circulation during the life-time of a vortex. As we have indicated earlier, the variation of position with time was very well approximated by a straight line which implies a constant convection velocity during each lifetime. The mean convection velocity of the vortices in the selfsimilar region is 724 cm/s with standard deviation 53 cm/s. The mean value is 5% higher than the mean of the free stream velocities 690 cm/s. The relatively large standard deviation results from the error introduced by the finite thickness of the braids. This error can be estimated as

$$\Delta U_c \doteq \frac{\Delta x U_c}{x}$$

where ΔU_c is the error in the convection velocity, Δx the error in the position (3 mm) and x/U_c the lifetime of the vortices. For $x = 4$ cm, ΔU_c becomes 53 cm/s.

The rate of change of the circulation during each lifetime in the selfsimilar region has a mean value of 2.5 cm/s and standard

deviation of 93 cm/s. This surprisingly large standard deviation may be entirely associated with the error from braid thickness which gives an estimated error in the circulation twice as large as in the position (i.e., 106 cm/s). This measurement and calculation were made in order to determine whether there are changes in circulation of the vortices during their lifetimes. Our conclusion is that, within the limitations of the measurement, there is no significant change in the mean value, but it is not clear how large any real variations may be because the relatively large error from finite braid thickness tends to obscure the results.

I.2.3 Evolution During Life-Span

A second motion picture obtained at a static pressure of 8 atm. and velocities of 1000 cm/s and 300 cm/s was used to gain some knowledge of the evolution of the parameters of the core during its life-span. A total of 20 frames were processed in which the vortex position and circulation as well as the core area and visual thickness were measured. An x-t diagram of the vortices involved is presented in figure I.9.

An estimate was made of the distance required to reach self-similarity from the results presented in table I.1. The high-speed-side boundary-layer thickness and Reynolds number at separation are

$$\theta_1 \sim .005 \text{ cm} \qquad R_{\theta_1} \sim 250$$

which give a transition distance of 1.5 cm, therefore all 155 vortices

in the sample (Fig. I.9) have reached the self-similar region. They correspond to 20 vortex time histories.

The growth of the mean circulation was obtained by fitting a straight line through the data in a least squares sense,

$$\overline{\ell} = 0.30\ (x - 0.0012)$$

Since $d\delta_\omega/dx = .097$ from Brown and Roshko (1974), $\overline{\ell}/\delta_\omega = 3.1$. The standard deviation normalized with the mean is 0.27 . Both results are in good agreement with previous measurements.

The core parameters D and A (see Fig. I.4) were measured for each of the 155 vortices in figure I.9. Since the circulation of each vortex is constant during its lifetime, it seems reasonable to assume that D and A will be proportional, at least as a first guess, to ℓ and ℓ^2 respectively. Simple averaging over all 155 samples gives $(\overline{D/\ell}) = 0.69$ and $(\overline{A/\ell^2}) = 0.49$, with standard deviations 0.16 and 0.18, respectively. These simple averages, however, do not give information about whether the cores grow during their lifetime. To study this we look for a relation between D/ℓ and $(x - x_0)/\ell \equiv \zeta$. Assuming a linear dependence of D/ℓ on ζ give the best fit line

$$D/\ell = 0.11\ \zeta + 0.31$$

with a standard deviation of 0.08. This line is shown in figure I.10. Only three of the 20 vortex time histories are shown, to give an idea of how well the line represents individual histories. If the vortices did not grow during their lifetimes, the line would be horizontal at the value $D/\ell = 0.69$. An important point is that the

line of course does not extend to $\zeta = 0$ and $\zeta = \infty$, because the vortices are formed and disappear at finite values of $(x - x_0)/\ell$ (see figure I.9). Our sample is too small to obtain meaningful mean values for these dimensionless positions which we call the mean formation value $\overline{\zeta}_F$ and the mean annihilation value $\overline{\zeta}_A$. The values which are indicated by ticks on the ζ-axis, namely $\overline{\zeta}_F = 2.4$ and $\overline{\zeta}_A = 4.8$, are deduced from the theoretical model discussed in chapter I.3.

Instead of the straight line in figure I.10, it would be possible to fit other curves, e.g., a square root dependence with time (i.e., with ζ) as suggested by Moore and Saffman (1975) to the data. The square-root assumption gives $D/\ell = 0.37\zeta^{\frac{1}{2}}$ with a standard deviation of 0.09 .

The growth of the vortex core area during lifetime was evaluated by assuming a linear dependence of A_c/ℓ^2 on ζ resulting in the relation

$$\frac{Ac}{\ell^2} = 0.13\ \zeta$$

with rms deviation from this line of 0.11.

This line is plotted in figure I.11 along with the same three vortex time histories used for comparison in figure I.10. Of significance is the fact that this best fit line goes through the origin; this result is in agreement with Moore and Saffman's suggestion for square-root growth rate (but here it implies extrapolation to $t = 0$). It also implies that there is little entrainment into the

vortex core during the amalgamation process; if we consider an amalgamation occurring at a downstream position x involving two vortices of circulation ℓ_1 and ℓ_2 and areas A_{c_1}, A_{c_2}, the newly formed vortex will have circulation $\ell = \ell_1 + \ell_2$ and area A_c given by

$$A_c = 0.13 \times \ell = 0.13 \times (\ell_1 + \ell_2) = A_{c_1} + A_{c_2}$$

Brown and Roshko (1974) used an estimate of the rate of change of the core area to calculate the entrainment velocities. Using our measurements we find

$$\frac{v_{e_1} + v_{e_2}}{U_1} = \frac{U_c}{U_1} \frac{1}{\ell} \frac{dA_c}{dx} = 0.085$$

This value is in relatively good agreement with the value 0.077 obtained by Brown (1974) from velocity measurements.

The agreement found between the entrainment rate calculated from the core area measurements and that obtained from velocity measurements indicated that the fluid engulfed by the large scale vortices eventually becomes part of the mixed fluid in the core. At high Reynolds number this process required the presence of smaller scale three-dimensional motions. In part II a mechanism is described involving the three-dimensional interaction between spanwise and streamwise vorticity which results in the growth of the large scale core.

The vortex visual thickness D can be used for comparison with the numerical results of Patnaik et al. (1976) who studied numerically the nonlinear development of the Kelvin-Helmholtz instability waves

at a Reynolds number of about 100. Their numerical solution when translated from their temporal solution to a spatially growing shear layer with $r = 0.3$ gives a visual growth rate defined by their density interface $d\delta_v/dx = 0.10$ which is in very good agreement with measurement of 0.11. On the other hand, the maximum value of their vortex core thickness is $D/\ell = 0.5$, which is about 50% lower than the values observed in our measurements. Of course the two situations are quite different; in one the diffusion of vorticity in the vortex and at its boundary is by viscous (molecular) mechanisms while in the other it is by (small scale) turbulence mechanisms, e.g., the streamwise vortices described in Part II.

Comparison can also be made with some conclusion about core parameters obtained by Moore and Saffman (1972, 1975) and by Pierrehumbert (1980). They found solutions of the steady Euler equations for an isolated vortex in a strain field and for a row of equal co-rotating vortices respectively, both with uniform vorticity cores. These solutions exist only for values of $A/\ell^2 < 0.27$ and $A/\ell^2 < 0.24$, respectively, where A is the area of the region containing vorticity. Our measurements however give $\overline{(A_c/\ell^2)} = 0.49$. The discrepancy may be associated with the vorticity distribution within A_c, which may not be uniform, with the streamwise nonuniformity in vortex size, non-steady effects or with three dimensional effects.

I.3 Statistical Theory of Vortex Circulation

The statistical theory of vortex circulation attempts to describe the self-similar probability distribution from their evolution properties. The implications of self-similarity are first introduced, they result in a common formulation of the Eulerian (constant x) and Lagrangian (constant ℓ) descriptions. The properties of the probability distribution are first studied in an Eulerian frame of reference where a conservation equation can be obtained. The results are then applied in the Lagrangian frame of reference. The arguments presented here are independent of velocity and denisty ratio, therefore the results apply to any value of these parameters. It also implies that no information can be obtained on the growth rate of the mean circulation since it depends upon those parameters.

I.3.1 Formulation

The self-similar vortex circulation distribution will be described by the probability of finding a vortex of circulation less than ℓ at a position less than x. Similarity requires it to be a function of $\xi = \ell/x$, thus

$$P(x_s \leq x; \quad \ell_s \leq \ell) = P(\xi) \qquad (I.3.1)$$

The amalgamation process will be characterized by two probability distributions, the probability that an amalgamation will result in the annihilation (P_A) or formation (P_F), respectively, of a vortex of circulation less than ℓ at a position less than x. Using the similarity scaling they can be written as

$$P_A(x_s \leq x, \quad \ell_s \leq \ell) = P_A(\xi)$$
$$P_F(x_s \leq x, \quad \ell_s \leq \ell) = P_F(\xi) \tag{I.3.2}$$

Associated with each of these probability distribution functions there is a probability density defined in the usual way

$$p(\xi) = \frac{dP(\xi)}{d\xi}$$
$$p_A(\xi) = \frac{dP_A(\xi)}{d\xi} \tag{I.3.3}$$
$$p_F(\xi) = \frac{dP_F(\xi)}{d\xi}$$

These probability density functions have two different physical interpretations. For an observer located at a fixed downstream position x, in the Eulerian frame of reference, they describe the probabilities of finding, of annihilation and of formation of a vortex of circulation $(\ell, \ell + d\ell)$, respectively. On the other hand, for an observer following vortices of circulation ℓ, in the Lagrangian frame of reference, they describe the probabilities that the event will occur at a position $(x, x + dx)$.

I.3.2 Eulerian Description

The number of vortices of circulation $(\ell, \ell + d\ell)$ being convected through a downstream location x per unit time is

$$n(\ell, x) = n_T(x)p(\xi)d\xi = n_T(x)\xi p(\xi)\frac{d\ell}{\ell} \tag{I.3.4}$$

where $n_T(x)$ is the total number being convected through it. The

function $n_T(x)$ can be obtained by considering the total length convected per unit time, which by definition equals the convection velocity U_c thus

$$n_T(x) = \frac{U_c}{\overline{\xi} x}$$
$$\overline{\xi} = \int_0^\infty \xi p(\xi) d\xi \qquad \text{(I.3.5)}$$

If the total number of vortices destroyed and formed by amalgamation per unit time at a position x are $n_A(x)$ and $n_F(x)$ respectively, the number destroyed and formed with circulation $(\ell, \ell + d\ell)$ are given by

$$n_A(x)\xi p_A(\xi) \frac{d\ell}{\ell}$$
$$n_F(x)\xi p_F(\xi) \frac{d\ell}{\ell} \qquad \text{(I.3.6)}$$

The combined effect of the amalgamation process is then

$$n_a(\ell, x)d\ell = [n_F(x)\ p_F(\xi) - n_A(x)\ p_A(\xi)]\ \xi \frac{d\ell}{\ell} \qquad \text{(I.3.7)}$$

An equation can be derived that relates $p(\xi)$, $p_F(\xi)$ and $p_A(\xi)$ by taking into consideration the conservation of vortex circulation during its life-span; that is, the change in $n(\ell, x)$ with x, keeping ℓ constant, equals the change due to amalgamation $n_a(\ell, x)$ or

$$\frac{\partial}{\partial x} n(\ell,x)d\ell = n_a(\ell, x)\ d\ell$$

which, after using equations (I.3.4), (I.3.5) and (I.3.7), gives

$$\frac{dn_T(x)}{dx} \left[\xi\ p(\xi) + \xi \frac{d}{d\xi} \left[\xi\ p(\xi) \right] \right] = \left[n_F(x)\ p_F(\xi) - n_A(x)\ p_A(\xi) \right] \xi \tag{I.3.8}$$

In order for this equation to be consistent it is required that

$$n_F(x) = - k_F \frac{dn_T(x)}{dx}$$

$$n_A(x) = - k_A \frac{dn_T(x)}{dx} \tag{I.3.9}$$

The constant k_F and k_A are both positive and represent the number of vortices formed and annihilated, respectively, per vortex lost during the amalgamation process. Using these definitions an equation relating $p(\xi)$, $p_A(\xi)$ and $p_F(\xi)$ is obtained:

$$\xi p(\xi) + \xi \frac{d}{d\xi} [\xi\ p(\xi)] = k_A\ \xi p_A(\xi) - k_F\ \xi p_F(\xi) \tag{I.3.10}$$

In order to solve this equation, it is convenient to introduce the function $g\ (\ell n\ \xi)$ defined as

$$p(\xi) \frac{d}{d\xi} g(\ell n\ \xi) = k_A p_A(\xi) - k_F p_F(\xi) \tag{I.3.11}$$

and the new variables $\alpha = \ell n\ \xi$ and $P(\alpha) = \ell n(\xi\ p(\xi))$. The equation (I.3.10) in these variables reads

$$1 + \frac{d}{d\alpha} P(\alpha) = \frac{d}{d\alpha} g(\alpha) \qquad \text{(I.3.12)}$$

which can readily be integrated to give

$$P(\alpha) = g(\alpha) - \alpha + k$$

The constant of integration k can be determined by the normalization condition on $p(\xi)$. Therefore, the general form of $p(\xi)$ consistent with similarity is

$$p(\xi) = \frac{e^{g(\ell n\ \xi)}}{\xi^2 \int_{\infty}^{\infty} e^{g(\alpha) - \alpha} d\alpha} \qquad \text{(I.3.13)}$$

The current understanding of the amalgamation process does not allow a determination of the function $g(\alpha)$. On the other hand, the exponential dependence of $p(\xi)$ on $g(\ell n\ \xi)$ suggests that the properties of $p(\xi)$ will be determined by the behavior of $g(\alpha)$ around its maximum α_0, which, in first approximation, depends quadratically on $(\alpha - \alpha_0)$ and therefore gives a lognormal distribution for $p(\xi)$, namely

$$p(\xi) = \frac{1}{\sqrt{2\pi}\ \sigma\xi} \exp\left\{ - \frac{1}{2\sigma^2} \left(\ell n \frac{\xi}{\overline{\xi}} + \frac{\sigma^2}{2} \right)^2 \right\} \qquad \text{(I.3.14)}$$

In this expression, $\overline{\xi}$ is the mean value of $\xi = \ell/x$, while the variance of ξ is $\overline{\xi}^2 (\exp \sigma^2 - 1)$ where $\sigma^2 = - \frac{1}{g''(\alpha_0)}$ (Aitchison and Brown, 1957). Comparison with experimental results is presented in figure I.8 for a value $\sigma = .276$. The agreement justifies the use of this appproximation through the rest of the discussion.

We turn our attention now to the width of distribution characterized by the parameter σ and its relation to the amalgamation process.

If $p(\xi)$ given by (I.3.14) is used in equation (I.3.10) it is found that

$$k_A p_A(\xi) - k_F p_F(\xi) = \frac{\sigma^2/2 - \ell n\, \xi/\bar{\xi}}{\sigma^2} p(\xi) \qquad \text{(I.3.15)}$$

If use is made of the fact that $p_A(\xi)$ and $p_F(\xi)$ are positive definite, they may be written in the convenient form

$$p_A(\xi) = \frac{1}{k_A}\left[\frac{\sigma^2/2 - \ell n\, \xi/\bar{\xi}}{\sigma^2} p(\xi)\, H(e^{\sigma^2/2} - \xi/\bar{\xi}) + q(\xi)\right] \qquad \text{(I.3.16)}$$

$$p_F(\xi) = \frac{1}{k_F}\left[\frac{\ell n\, \xi/\bar{\xi} - \sigma^2/2}{\sigma^2} p(\xi)\, H(\xi/\bar{\xi} - e^{\sigma^2/2}) + q(\xi)\right]$$

where H is the unit step function and $q(\xi)$ is a positive-definite function.

The functions $p(\xi)$, $p_A(\xi)$ and $p_F(\xi)$ are sketched in figure I.12 for $q(\xi) \equiv 0$. The basic feature described by these equations is that for $\xi < \bar{\xi}\, e^{\sigma^2/2}$ vortices are destroyed by the amalgamation process $(p_A(\xi) > 0,\ p_F(\xi) = 0)$. The resulting vortex formed by the amalgamation has $\xi > \bar{\xi}\, e^{\sigma^2/2}$ $(p_A(\xi) = 0,\ p_F(\xi) > 0)$. It is this transfer of vortices through $\xi = \bar{\xi}\, e^{\sigma^2/2}$ that determines the probability distribution $p(\xi)$. Amalgamations not involved in this transfer are described by the function $q(\xi)$ which does not affect the probability distribution.

The normalization condition on p_A and p_F results in the equations

$$k_A = I(\sigma) + K$$
$$k_F = I(\sigma) - 1 + K \qquad \text{(I.3.17)}$$

where

$$K = \int_0^\infty q(\xi)\, d\xi$$

and

$$I(\sigma) \equiv \frac{e^{-\sigma^2/2}}{\sqrt{2\pi}\ \sigma} + \text{erf}\ (\sigma) \qquad \text{(I.3.18)}$$

k_A and k_F are defined by equations (I.3.9). Since $\frac{dn_T(x)}{dx} = n_F(x) - n_A(x)$, $k_A - k_F = 1$ and therefore the equations in (I.3.17) are not independent. The values of k_A and k_F are determined by the amalgamation process. In tearing, three vortices are destroyed and two formed, therefore $k_A = 3$ and $k_F = 2$; similarly, in pairing, $k_A = 2$, $k_F = 1$ and in tripling $k_A = \frac{3}{2}$ and $k_F = \frac{1}{2}$.

An additional assumption is needed concerning K in order to solve equation (I.3.17) for σ. As a first guess the equation (I.3.17) was solved for $K = 0$ and the above three forms of amalgamation, tearing, pairing, and tripling. These results are given in Table I.2.

Using the value $\sigma = 0.276$ found for pairing, the standard deviation $\bar{\xi}\ (\exp \sigma^2 - 1)^{\frac{1}{2}}$, normalized by $\bar{\xi}$, is found to be 0.28 in good agreement with the measured values of 0.24 for $s = 1$ found in

this investivation and 0.31 reported by Brown and Roshko (1974) for s = 7.

This result implies that coalescence by pairing is the dominant form of interaction, which agrees with our observations. The presence of other forms of amalgamation as well as $q(\xi) \neq 0$ can modify slightly the value of σ. Tearing results in a smaller standard deviation while tripling gives a larger value compared with the value for pairing. The effect of $q(\xi) \neq 0$ is to increase the standard deviation for a given form of amalgamation.

The result of this study is that the self-similar probability distribution of large scale vortex circulation is a lognormal distribution with a standard deviation of 0.28 independent of velocity and density ratio. Comparison is made in figure I.8 with experimental measurements in a constant density mixing layer presented in the previous chapter and for a density ratio $s = 7$ made by Brown and Roshko (1974). The agreement is excellent, in particular the location of the peak, i.e., the mode of the distribution, is well characterized by this theory. Also plotted in the figure are the results of Takaki and Kovasznay (1978), who found a wider distribution with the mode at a smaller value of $\ell/\overline{\ell}$.

I.3.3 Lagrangian Description

The results obtained in the previous section provide some information on the Lagrangian description of vortex evolution. The different probability density functions will be presented in terms of the similarity variable $\zeta = x/\ell$ used in describing the vortex parameters in section I.2.3.

The probability of finding a vortex of circulation ℓ at a position $(x, x + dx)$ is given by $p(\xi)\, d\xi$ which, after change of variable, becomes

$$p_\zeta(\zeta)d\zeta = \frac{1}{\sqrt{2\pi}\,\sigma} \exp\left\{-\frac{1}{2\sigma^2}\left(\ell n\ \zeta/\bar{\zeta} + \frac{\sigma^2}{2}\right)^2\right\} d\zeta \qquad \text{(I.3.19)}$$

with $\bar{\zeta} = e^{\sigma^2}/\bar{\xi}$. Its maximum value is found at $\zeta_M = \bar{\zeta}e^{-3\sigma^2/2}$. The probability of formation $p_F(\xi)$ and annihilation $p_A(\xi)$ after change of variable and neglecting $q(\xi)$ read

$$p_F(\zeta)d\zeta = -\frac{3\sigma^2/2 + \ell n\ \zeta/\bar{\zeta}}{[I(\sigma) - 1]\sigma^2}\, p_\zeta(\zeta)\, d\zeta \qquad 0 < \zeta/\bar{\zeta} < e^{-3\sigma^2/2}$$

$$p_A(\zeta)d\zeta = \frac{3\sigma^2/2 + \ell n\ \zeta/\bar{\zeta}}{I(\sigma)\sigma^2}\, p_\zeta(\zeta)\, d\zeta \qquad e^{-3\sigma^2/2} < \zeta/\bar{\zeta} < \infty$$

(I.3.20)

$p_\zeta(\zeta)$, $p_F(\zeta)$ and $p_A(\zeta)$ are sketched in figure I.13. The interpretation of these probability distributions is readily found. If we consider vortices with a given circulation ℓ, $p_F(\zeta)$ indicates that they are formed by coalescence until a downstream position $x = \zeta_M \ell$ is reached. From that point amalgamation gradually destroys the vortices of this circulation as indicated by $p_A(\zeta)$.

The functions $p_F(\zeta)$ and $p_A(\zeta)$ can be used to obtain the mean formation and destruction locations, $\bar{\zeta}_F$ and $\bar{\zeta}_A$, defined as

$$\overline{\zeta}_F = \int_{\theta}^{\overline{\zeta}_e e^{-3\sigma^2/2}} \zeta \, p_F(\zeta) \, d\zeta = 2 \, \overline{\zeta} \, \frac{I(2\sigma) - 1}{I(\sigma) - 1} \tag{I.3.21}$$

$$\overline{\zeta}_A = \int_{\overline{\zeta}_e e^{-3\sigma^2/2}}^{\infty} \zeta \, p_A(\zeta) \, d\zeta = 2 \, \overline{\zeta} \, \frac{I(2\sigma)}{I(\sigma)}$$

where the function $I(\sigma)$ is given by equation (I.3.18). The values of $\overline{\zeta}_F/\overline{\zeta}$ and $\overline{\zeta}_A/\overline{\zeta}$ for the three forms of amalgamation cosidered are given in table I.2, as well as the mean life-span $\overline{L}$ of the vortices normalized with their mean life-span position X,

$$\frac{\overline{L}}{X} = 2 \, \frac{\overline{\zeta}_A - \overline{\zeta}_F}{\overline{\zeta}_A + \overline{\zeta}_F} \tag{I.3.22}$$

The value for pairing $\overline{L}/X = 0.67$ can be compared with the measurements of Brown and Roshko (1974), $\overline{L}/X = 0.39$, and of Hernan and Jimenez (1979), $\overline{L}/X = .61$. The theoretical result overestimates slightly the experimental values, the presence of other forms of amalgamation and some overlap may account for some of the discrepancy but it should also be pointed out that the experimental samples were small.

Comparison can also be made with the experimental results presented in figure I.10 and I.11 of the vortex evolution. For that

sample, $\overline{\xi} = 0.3$ and $\sigma^2 = .07$ which gives $\overline{\zeta} = 3.6$, $\overline{\zeta}_F = 2.4$ and $\overline{\zeta}_A = 4.8$. These mean values are consistent with the measured evolution of the three vortices presented in the figures.

I.4 Summary

In this investigation we have used the properties of an ensemble of large scale vortices to characterize the transition region and the subsequent self-similar behavior of the flow. A model of the statistical distribution of vortex strength (circulation) was also developed that provides additional insight into the dynamics of the self-similar evolution.

A summary of the results follows.

(1) The extent of the transition as determined in this investigation on the basis of vortex similarity is in good agreement with previous measurements. In the transition region the mean circulation increases monotonically while the rms reaches a peak within the region.

(2) In the fully developed turbulent region the mean circulation normalized with the vorticity thickness is $\overline{\ell}/\delta_\omega = 3.0$ and the rms fluctuation normalized with the mean is $\ell'/\overline{\ell} = 0.24$.

(3) The evolution of the normalized core parameters, the visual thickness D/ℓ and area A_c/ℓ^2 are adequately described in terms of the similarity variable $(x - x_0)/\ell \equiv \zeta$. The scatter of the measurements was too large to choose between a square root dependence of D/ℓ on ζ or a linear one (with non-zero origin); the former gives

$$\frac{D}{\ell} = 0.37\ \zeta^{\frac{1}{2}}, \qquad \frac{A_c}{\ell^2} = 0.13\ \zeta$$

This functional dependence was suggested by Moore and Saffman (1975). The rms deviations from these lines, 13% for $(\overline{D/\ell})$ and 22% for

$(\overline{A_c/\ell^2})$ respectively, are about the same as the resolution of the measurements. That is, any possible effects of initial conditions (at formation of the vortices) are smaller than the resolution of the measurement.

(4) The statistical theory of vortex circulation presented in Chapter I.3 adequately describes the shape and variance of the probability distribution. It is a lognormal distribution with a parameter σ which is independent of velocity and density ratio. The assumptions upon which this result was obtained are

i. Self-similarity. The probability distributions are only a function of the similarity variable $\xi = \ell/x$.

ii. The vortex circulation is conserved during its evolution.

iii. The dependence of the amalgamation process on the circulation of the vortices involved is such that the function $g(\alpha)$ can be approximated by

$$g(\alpha) = -\frac{1}{\sigma^2}(\alpha - \alpha_0) + a(\alpha - \alpha_0) + b$$

iv. The overlap function $q(\xi) \equiv 0$. It implies that for a given value of ξ amalgamation can either form or destroy vortices but not both.

Because of the third assumption the lognormality of the distribution should formally be interpreted as a first term in an expansion with small parameter $\varepsilon = \sigma^3 g'''(\alpha_0)$.

The numerical value of σ depends on the type of amalgamation assumed; if pairing is the dominant form then $\sigma = 0.276$, which agrees best with the experimental value.

(5) The statistical theory also gives the mean formation and annihilation positions of the vortices. These results are consistent with the limited evidence available. The mean life-span normalized with the mean position $\overline{L}/X = 0.67$ is in reasonable agreement with experimental measurements.

Part II

SECONDARY STREAMWISE VORTEX STRUCTURE

II.1 Introduction

The measurements reported in this part were motivated largely by some results of earlier experiments made at GALCIT, notably those of Konrad (1976) and Breidenthal (1978), both of whom noted on plan views of the mixing layer the presence of streamwise streaks which were clearly associated with the development of three-dimensional motions. Both of them also described a mixing transition region in which the internal mixedness of the shear layer increases and which was associated with the development of the streak pattern. It was speculated that the streaks delineated streamwise vortices which contributed to the increased mixing, either directly and/or after further instability.

The experiments described in this part were done in the gas Brown-Roshko facility used by Konrad as well as in Breidenthal's water facility. It was our objective to obtain a beter understanding of the origin and nature of the structure associated with the streamwise streak patterns. We approached this by first observing the effects of apparatus and flow parameters on the streak pattern early in its history. Screens in the settling chamber of the gas mixing facility and the length of the splitter plate were changed; Reynolds number and velocity ratio were varied. Time exposure pictures indicated a spanwise mean structure which was then investigated further by means of concentration probes. These clearly indicated that indeed the streaks are associated with streamwise vortices. Finally, direct visualizations of those vortices were obtained in the water facility

and high speed movies made it possible to obtain a description of their spatial relation to the primary spanwise vortices. The implications of changes of scale observed in the concentration measurements, and evident on the earlier pictures of Konrad, are discussed.

II.2 Helium-Nitrogen Mixing Layer Results

The Brown-Roshko (1974) gas facility was used to study the three-dimensional structure of the mixing layer between helium and nitrogen streams. Flow visualization and concentration measurements were the principal experimental techniques utilized in this investigation. A brief description of the apparatus and experimental techniques, followed by the flow visualization results and concentration measurements, will be presented.

II.2.1 Apparatus and Experimental Techniques

The gas mixing layer facility is a two-channel pressurized, blow-down tunnel. The gases are stored in high-pressure bottles, eight bottles for each channel. Two independent lines, which include a pressure regulator, a metering valve and a remotely operated ball valve, provide an adjustable mass flow for each channel. The working section is enclosed in a high pressure vessel, whose pressure is maintained at the required level by a regulator.

In each channel, the gas flow enters an entrance section which contains several turbulent reducing elements, namely a 0.64 cm thick foam, a perforated plate with 44% open area ratio, a 4 cm long honeycomb section with 0.2 cm cell size and a fine mesh screen with 50% open area ratio. After that the flow enters a two dimensional contraction with 4 to 1 area ratio. The resulting free stream

turbulence level is below 0.5%. The two channels are separated by a splitter plate which terminates at the entrance to the test section in a 6 degree wedge.

The test section is rectangular in cross-section, 5 cm high by 10 cm wide. At the entrance each free stream occupies one half of the cross-section, i.e., 10 cm x 2.5 cm, the larger dimension being spanwise. The top and bottom walls, those parallel to the mixing layer, are adjustable so that the pressure gradient in the flow direction can be minimized. The length of the test section is 25 cm, but only the initial 11 cm was used in the measurements.

Shadowgraph and schlieren flow visualization was used in these experiments. The optical system is sketched in figure II.1. It is based on the system described in Part I. Simultaneous side and plane views were obtained with two first surface flat mirrors as shown in the figure. In the schlieren system the knife edge was positioned parallel to the flow direction, thus the intensity pattern on the film is proportional to the density gradient across the layer in the side view and along the span in the plan view, respectively. A stroboscopic light source, the Genrad 1538A, was used for the schlieren pictures. Time exposures were obtained by strobing the unit at 100 Hz for 2 seconds.

Concentration measurements were made using the probe developed by Brown and Rebollo (1972). The probes were calibrated in a

different facility against a mixture of known composition. Power spectrum measurements of the concentration fluctuation showed no appreciable energy content above 15 kHz. At the velocities used, this value corresponds to a spatial resolution of 0.2 mm.

Two concentration probes and one pitot-static probe deployed at fixed positions along the span, were used in most data acquisition runs. During each run the set of three probes was traversed normal to the shear layer, stopping at 21 points within the layer. The position accuracy was 0.02 cm. At each stopping point the probes' output was digitized sequentially at a combined rate of 96 kHz for 0.18 seconds and stored on digital tape for later processing. The data acquisition and digital operations were performed with a computer-controlled data acquisition system called the "Solo System."

The mean and rms fluctuations of the concentration was obtained from these data. In addition, molecular mixing was characterized by computing the amount of product formed in the layer by an hypothetical infinitely fast irreversible chemical reaction. Under the assumption of equal diffusion coefficients of all the species involved the amount of product, normalized by the concentration of the reactant carried by the low speed fluid, is (Toor 1962, Konrad 1976)

$$\tilde{C}_p = \frac{C_p}{C_{B_0}} = \frac{C}{f} \qquad 0 < C < \frac{f}{1+f}$$

$$\tilde{C}_p = 1 - C \qquad \frac{f}{1+f} < C < 1$$

where C, C_p, C_{B_0} and C_{A_0} are the helium, product and free stream reactant concentrations, with $f = C_{B_0}/C_{A_0}$. A single value of $f = 3$ was used in this investigation to characterize molecular scale mixing. This value was also used by Konrad (1976), hence comparison can be made with his detailed measurements at a fixed spanwise position.

II.2.2 Flow Visualization Results

Quantitative data on the onset of the streamwise vortices was obtained from flow visualization pictures. Figure II.2 shows two visualizations of a mixing layer with U_{He} = 496 cm/s , r = 0.5, p = 4 atm. (a) shows an instantaneous (1-2 μsec) spark schlieren picture, while (b) is obtained from a 2 second exposure. It may be seen that the position of the streamwise streaks in the two pictures is the same, implying that there is little fluctuation in their spanwise positions.

The persistence of the streaks at fixed spanwise positions suggests that they may be associated with disturbances originating somewhere upstream in the settling chamber. Indeed, changes in the screens produced changes in their spanwise positions. On the other hand, it is clear that the flow disturbances associated with the streaks are being amplified from their upstream origins until they reach levels at which they become visible on the photographs. The location of this visible threshold amplitude could be shifted upstream or downstream by raising or lowering the Reynolds number (for fixed velocity ratio). These flow changes also changed the

number of streaks. For example, figure II.3 shows pictures obtained under exactly the same experimental conditions as figure II.2, except for a change of velocities as indicated. It may be seen that there is a considerable change in the streak pattern. Our conclusion from these and other comparisons, discussed below, is that the streaks are associated with true flow instabilities which, of course, originate from the available upstream disturbances, but which respond differently to different flow conditions. In particular, we studied the dependence of the mean spacing and the beginning of the visible pattern on the flow parameters.

An appropriate reference length for the spanwise spacing of the streaks might be the initial thickness of the shear layer after it leaves the splitter plate. Apart from the difficulty of measuring this small thickness, there are well known problems of defining the position of initial thickness, compounded here by the fact that the shear layer is generated from initial boundary layers in two different gases. Therefore, we use for the reference length the wave length of the initial Kelvin-Helmholtz instability wave λ_{2Di} which can easily be measured on the photographs. In a sense, this instability wave educes the appropriate length parameter and provides a convenient means of measuring it.

Using the time exposures, measurements were made of the distance x_{3D} to the visual origin of the pattern, of the spacing λ_{3D} and of the visual thickness δ_{v_0} of the layer at x_{3D}. Instantaneous

pictures were used to measure the streamwise (Kelvin-Helmholtz) wavelength λ_{2Di} of the initially rolled-up laminar shear layer and also λ_{2D_0} at x_{3D}. (λ_{2D_0} is always greater than λ_{2Di} because amalgamations have occurred before the onset of the visible pattern. The values of both lengths are actually average values from two realizations of the flow.) The results of the measurements are summarized in table II.1, where the layer thickness at the beginning of the pattern is characterized by what we call the onset Reynolds number $\Delta U \delta_{v_0} / \nu_{N_2}$, while the spanwise mean spacing and its rms fluctuation are normalized by λ_{2Di} and λ_{2D_0}.

These results are presented in figures II.4 and II.5 for the onset Reynolds number and the mean spacing, respectively. We have used in these figures the parameter $\Delta U/U_c$ instead of the velocity ratio r, where ΔU is the difference in free stream velocities and U_c is the convection velocity of the large vortices. Its relation to the velocity and density ratio is according to Brown (1974)

$$\frac{\Delta U}{U_c} = \frac{(1 + s)(1 - r)}{1 + sr}$$

As shown in figure II.4 the onset Reynolds number depends strongly on this parameter changing by a factor of 4 over the range 0.8 to 2.2, which corresponds to a change in r from 0.15 to 0.5. The extension of the partition resulted in an increase of the onset Reynolds number for the same velocity ratio. We believe that this is due to a change in boundary-layer profile shape.

The mean spanwise spacing λ_{3D}, normalized with the streamwise wavelength at onset, λ_{2D_0}, is plotted as a function of the parameter $\Delta U/U_c$ in figure II.5. The error bars give the rms variation calculated using all the data at a particular value of $\Delta U/U_c$. No significant trend with $\Delta U/U_c$ is apparent and therefore the mean and rms were calculated using all samples available, which gives

$$\frac{\lambda_{3D}}{\lambda_{2D_0}} = .67 \quad , \qquad \frac{\lambda'_{3D}}{\lambda_{2D_0}} = 0.43$$

The large rms deviation is not surprising because individual realizations have rms variations as high as 0.3 (see table II.1).

The time exposure pictures show significant downstream deterioration of the coherent streamwise pattern at sufficiently high Reynolds number, as in figure II.3. In these cases the evolution is characterized by a gradual loss of contrast and by spacing changes. Additional evidence of this was obtained from high speed shadowgraph motion pictures. They showed that the spanwise location of the streaks is initially fairly well fixed, but further downstream variations in the pattern develop. The lateral positions of the streaks at a given downstream location fluctuate in time and the number of streaks across the span decreases with increasing distance downstream. This behavior is consistent with the time exposure pictures since the lateral displacement and spacing changes will result in loss of the initial coherence of the pattern. In all flow conditions considered in this investigation the streamwise streaks were observed in instantaneous

pictures even at the downstream end of the test section, downstream of the mixing transition, up to the highest Reynolds number.

II.2.3 Concentration Measurements

The streamwise streak pattern evident in the time exposures indicated the existence of persistent spanwise concentration gradients in the spanwise direction indicating that there are spanwise non-uniformities in the mean flow. The concentration measurements were undertaken to obtain quantitative definition of these nonuniformities and to provide some insight into the underlying structure that generates them. Also we wished to see whether any mean spanwise structure actually remains in regions downstream of where it has disappeared from the time exposure pictures. The measurements were limited to the case with free stream velocity of 1000 cm/s on the helium side, 380 cm/s on the nitrogen side and test section pressure of 6 atmospheres. These conditions $s = 7$ and $r = 0.38$ were chosen so that comparison could be made with the results of Brown and Roshko (1974) and Konrad (1976).

In order to establish a basis for comparison with those previous measurements, traverses were made with a single probe positioned at midspan. The concentration thickness defined as the distance across the layer between points where the mean concentrations are 0.01 and 0.9 was found to follow the expected linear dependence on downstream distance

$$\delta_{0.01} = 0.22\ (x - x_0), \qquad x_0 = -\ 1.58 \text{ cm}$$

The growth rate 0.22 is in good agreement with the results of Brown and Roshko (1974). The value of x_0 is used to define the similarity variable $\eta = y/(x - x_0)$.

Once the correspondence with earlier results had been established, we proceeded to measure spanwise variations by using two concentration probes, one of them positioned at midspan ($z = 0$) and the other at various spanwise positions z. The downstream evolution of the mean concentration profiles differs, depending upon spanwise position. With the two probes spaced 0.64 cm, pairs of profiles were obtained at four downstream stations as shown in figure II.6. The spacing was chosen on the basis of time exposure pictures so that both probes were located at neighboring streaks, consequently the close agreement found at $x = 3$ cm is to be expected. As the probes were moved downstream, keeping their spacing constant, differences in the mean concentration profiles developed. As will be seen later, this is due to an increase in the mean spacing of the streaks and they no longer correspond to the probe spacing.

To study this more completely, the mean concentration and its rms fluctuation were mapped over part of the cross-sectional (y-z) plane, at two downstream locations, $x = 4$ cm and $x = 9$ cm. The results are plotted in figures II.7 and II.8, respectively. At the upstream location, the spacing of the peaks (or of the valleys) corresponds to the streak spacing in the time exposure pictures. For the mean concentration, the peaks are in phase (spanwise) all across the layer while for the rms fluctuation peaks on the helium side are

in phase with valleys on the nitrogen side. For the latter the change over occurs at approximately $\eta = -0.08$ which corresponds to the position in the profile where the spanwise oscillation of $\overline{C}$ has its maximum amplitude. It is also evident that peaks and valleys in $\overline{C}$ are lined up with those in C'.

Further downstream at x = 9 cm (figure II.8) the same features are evident but the spanwise spacing between peaks and valleys has increased. Using the spanwise spacing defined by the central part of the figure gives the normalized value $\lambda/\delta_\omega = 1.0$ in terms of the local vorticity thickness (Konrad's value). Nearly the same dimensionless value is obtained at the upstream station (x = 4 cm) when an average value for λ is calculated from the three wavelengths available in figure II.7. Between x = 4 cm and x = 9 cm the change in scale is by a factor of 1.9 in δ_ω and, evidently, the same for the spanwise structure. As will be seen in figure II.12, the two stations are just upstream and downstream, respectively, of the mixing transition. The amplitude of the spanwise oscillations of the mean concentration is not strongly affected by downstream position; its maximum rms variation of 0.10 occurs at $\eta \doteq 0.07$. The maximum fluctuation in time, whose rms value is $C' = 0.30$ occurs at the same value of η but as noted before, has little spanwise variation.

Some insight into the mean spanwise variation can be obtained by comparing simultaneous concentration time histories from the two probes. This is illustrated in figure II.9 where the concentration

histories measured by the two probes at $x = 9$ cm, $z = 0$ and $z = 0.64$ are shown at three locations across the layer. At the center of the layer, $\eta = -0.04$, large concentration fluctuations associated with the large scale vortices dominate the signal. These large fluctuations appear almost simultaneously in time indicating the basic two-dimensionality of the large scale structures. There are, however, differences in the smaller amplitude, higher frequency fluctuations which are superimposed on the large ones. At the edges, $\eta = -0.09$ and 0.04, there is in general a correlation between large spikes in the two signals but their shapes and deviations are not so consistently similar as at the center of the layer and occasionally one probe shows no evidence of the passage of the vortex seen at the other probe only 0.64 cm away. This spacing is equal to approximately half the vorticity thickness at this location! Clearly there are large changes in the internal structure of the large, spanwise vortices. As will also be confirmed by the pictures in Chapter II.3, this internal structure results in significant distortions of the large vortices but their overall spanwise coherence is preserved.

The concentration histories were also used to calculate the amount of chemical reaction product (Konrad 1976). The mean product formed as a function of span and position across the layer is plotted in figure II.10 for $x = 4$ and 9 cm. Its behavior is similar to that of the rms of the concentration, fluctuation, with a 180° phase change across the layer; the position at which this change occurs is $\eta = -0.04$, different from the value found for the rms.

The product thickness defined as

$$\delta\tilde{C}_P = \int_{-\infty}^{\infty} \tilde{C}_P(y)\, dy$$

is plotted versus span for the two downstream positions in figure II.11. The low amplitude of the oscillations results from the observed phase change across the layer. The product thickness dependence on downstream distance is presented in figure II.12 for two spanwise positions $z = 0$ and $z = 0.64$ cm. Also plotted in the figure are the measurements of Konrad (1976). The measurements at $z = 0$ show good agreement with those of Konrad, in particular, the mixing transition is observed at the same Reynolds number. The measurements at $z = 0.64$ cm show a smaller amount of mixing.

Comparison was also made between the result of Konrad and our own with the time exposure pictures. Shown in figure II.13 is a time exposure picture together with a plot of the product thickness growth rate $\delta\tilde{C}_P/(x - x_0)$ versus large scale Reynolds number $\Delta U\delta_\omega/\nu_{N_2}$ where δ_ω is given by

$$\delta_\omega = 0.119\ (x - x_0)$$

from Konrad (1976). The plot and picture have the same horizontal scale. It is observed that the mixing transition occurs at approximately the downstream location where some of the streaks in the picture merge, resulting in the scale change.

II.3 Constant Density Mixing Layer

II.3.1 Apparatus and flow visualization technique

The water mixing layer facility designed by Breidenthal (1978) was used in flow visualization experiments using laser-induced fluorescence. It is a gravity driven apparatus in which the free stream fluid is supplied from two independent reservoirs located one floor above the test section. Although the facility is designed to operate at higher velocities a maximum velocity of 100 cm/s was used in these experiments.

The technique of laser-induced fluorescence, which was developed in this laboratory by Professor P.E. Dimotakis, was used for flow visualization. The fluorescent dye fluorescein was dissolved in one free stream. A plane sheet of light was used to excite its fluorescence which was recorded with conventional photographic techniques. The sheet was obtained from an argon-ion laser and had a thickness less than 0.5 mm. A similar system has been used by Dewey (1976).

The cross-sectional flow pictures described in the next section were obtained with the plane of illumination perpendicular to the free stream velocity. Because of geometrical limitations in the facility the photographic and motion picture camera optical axis formed an angle of approximately 30° with the perpendicular to the visualized plane, which resulted in some distortion of the pictures.

II.3.2 Flow visualization results

Two cross-section pictures of the mixing layer at a Reynolds number of $\Delta U \delta_\omega / \nu \doteq 3 \times 10^3$ are shown in Figure II.14. The flow is

perpendicular to the plane of the picture and toward the viewer. The high speed stream is at the top and the low speed stream, carrying labeled fluid, is at the bottom. Figure II.14(a) is a cross-section through a large scale primary vortex core while figure II.14(b) is a cross-section through a braid. Even though the technique does not visualize vorticity, the presence of streamwise counter-rotating vortices is inferred from the swirled interface.

The expected changes resulting from the primary vortex structure are readily observed in these pictures. The braid is a region where fresh free stream fluids meet, resulting in a sharp contrast change, while in the core there is a region of mixed fluid separating the free streams. The streamwise vortex structure also shows significant variations in the two regions. In a cross-section through the core, a row of counter-rotating vortices stretching across the span is observed at both sides of the mixed region while the cross-section through the braid has a single row of streamwise vortices. (The properties of such streamwise vortices in a braid have been investigated by Corcos, 1979.)

The peculiarities of the streamwise vortex structure and its interaction with the primary vortices was further investigated with a high speed motion picture obtained at a Reynolds number $\Delta U\delta_\omega/\nu = 2.4 \times 10^3$. Three sequences from this movie, shown in figures II.15, II.16 and II.17 will be discussed in the following paragraphs. It may be helpful in following the discussion to refer to figures II.18(a), (b), (c), which were constructed on the basis of these and other movie sequences.

The sequence in figure II.15 shows the passage of a primary vortex through the visualized plane. In the first two pictures the preceding braid is seen to move toward the low speed side, and the streamwise vortices follow this motion. First contact of the primary vortex core with the plane of visualization is seen in the third frame (t = 0.1 sec). It occurs at isolated regions along the span indicating outflow of fluid from the core in these areas; furthermore these outflow regions correlate well with the counter-rotating vortices at the low speed side, in particular with the positions where their induced velocity field is directed upwards.

As the core moves through the visualized plane a row of counter-rotating vortices appears on the high speed side. Vortex pairs on the high and low speed sides of the primary vortex are aligned with each other in such a way that they have the same sign of vorticity at the same spanwise location. Another feature of the streamwise and primary vortex interaction is the tendency of the streamwise vortices to move away from the core. This trend can also be observed in figure II.14(a).

The subsequent evolution shows the streamwise vortices at the low speed side disappearing with the primary vortex core leaving behind a region of outward flow from the core (t = 0.35) i.e., normal to the picture plane upstream. The streamwise vortices at the high speed side continue through the trailing braid, following it as it moves towards the low speed side.

The outflow region observed prior to the appearance of the streamwise vortices on the high speed side and after the disappearance of those at the low speed side indicates that the streamwise vortices bend around the periphery of the large scale vortex core.

No evidence was found of the continuation of the streamwise vortices along the periphery of the primary vortex beyond the regions where the vortex lines are perpendicular to the plane of the mixing layer, which suggests that the vortices in each counter-rotating pair join in a hairpin configuration. Although direct evidence of the presence of the hairpins was not obtained this conjecture is consistent with the observations by Breidenthal (1978) of the early development of three-dimensionality; he found that stretching of a primary vortex core oscillation (the "wiggle") leads to the formation of the streamwise vortices.

A slightly different evolution is observed in figure II.16 where the same streamwise vortices at the low speed side persist through two primary vortices. An interesting interaction occurs after the first primary vortex has moved through the visualized plane (t = 0.4 to 0.5 sec). The streamwise vortices at the low speed side and those in the intervening braid appear to retain their identity until the second vortex moves through the plane. This behavior can be associated with pairing of the two primary vortices.

The sequence in figure II.17 follows the streamwise vortices between neighboring primary vortices. The sequence begins at a primary vortex core. The streamwise vortices are first seen at

t = 0.05, in particular, a counter-rotating pair on the high speed side slightly to the right of the center of the picture. As the primary vortex moves across the visualized plane the two vortices in the pair separate. The lateral motion receeds somewhat as the vortices move with the braid to the low speed side. The process accelerates as the streamwise vortices reach the low speed side of the trailing primary vortex. This behavior is associated with the curvature imposed on the path of the streamwise vortex pair by the primary vortex velocity field. Furthermore, this curvature induces a precessional motion which results in uneven spacing between the streamwise vortices on the periphery of the primary vortex and therefore to a mutually induced radial velocity directed outwards.

These induced motions outward from the core may be the main contributions to the observed growth between pairings of the primary vortices, described in Part I. As the counter-rotating pairs move away from the core, their induced velocity field carries mixed fluid from the core outward while it brings in fresh irrotational fluid.

Based on these pictures the idealized diagram of the vortex lines presented in figure II.18 was constructed. A streamwise vortex segment is part of a continuous line which loops back and forth between adjacent primary vortices as shown in figure II.18(a). Thus on successive passes, its streamwise direction changes sign, forming the vortex pairs that are seen in the cross section views. These warp-like structures, linking adjacent pairs of primary vortices, align themselves with each other so that, in plan view they appear to be

straight streamwise streaks. Actually, in the ideal picture the projections onto a plan view would not really be continuous but would have deflections, above and below the primary vortices as shown in figure II.18(c), due to the induced precessional motions described above. On shadow and schlieren pictures, these details, superimposed on other features from the internal structure of the primary vortex, are obscured.

In figure II.19 is a sequence from a high speed motion picture obtained at a Reynolds number $\Delta U\delta_\omega/\nu = 10^4$ which, according to the results of Breidenthal (1978), is downstream of the mixing transition. The reasons for the poorer resolution in this sequence are not entirely clear, but it is probably simply due to poorer focussing resulting from the wider aperture that had to be used at this higher flow speed. The figure shows the passage of a braid through the visualized plane. The streamwise vortices can be followed along the braid. Their spacing is smaller than in previous pictures since the higher velocity results in a thinner initial shear layer, which determines their spacing.

II.4 Discussion and Conclusions

Perhaps the most striking result of this investigation is the elucidation of the streamwise vortex structure and its spatial relation and interaction with the primary spanwise vortices. An idealized sketch is given in figure II.18. Unlike previous interpretations of the streak patterns, that each streamwise vortex is unidirectional, it may now be seen that it is part of a warped vortex line threading its way up- and downstream between any two adjacent primary, spanwise vortices, thus changing its streamwise directional sign on each pass. This structure is first established after the Kelvin-Helmholtz instability has developed into spanwise coherent vortices, possibly as early as the first pairing. The "wiggle" described by Breidenthal (1978) is its first manifestation.

As defined by the time exposure pictures, the mean onset Reynolds number was found to decrease as the velocity ratio increase, i.e., as the mixing layer approaches a wake. These results indicate that an initial profile containing a wake component is more unstable to three dimensional disturbances. Also determined from the time exposures, the mean spanwise spacing of the streaks, normalized by the mean local spacing of the primary vortices, is independent of velocity ratio and equal to 0.67. This is equal to the most amplified spanwise wave length found by Pierrehumbert (1980) in his computation of the translative instability of a row of Stuart vortices. The scatter in the measurements is consistent with the broad amplification curve. As pointed out by Pierrehumbert the

shallow peak is also consistent with the fact that, once formed, the structure preserves its spanwise scale for some distance downstream, through one or two additional pairings.

The proposed warped vortex line structure was inferred mainly from a frame-by-frame study of cross sectional movies. It is also consistent with the concentration measurements, which show that, associated with this structure, there is a well defined spanwise entrainment pattern. The fluid from the high and low speed side is entrained at different spanwise positions. The fluids are mixed in the primary vortex core and the resulting mixture is pulled outwards at different spanwise positions. The rms of the concentration fluctuation and the mean mixing product show similar features consistent with the pattern described above.

The observed pattern should also have an effect on the spanwise velocity distribution. In regions where high speed fluid is entrained a larger momentum is expected. Measurements by Jimenez et al. (1979) show precisely this effect, although their interpretation is somewhat different from ours.

The concentration measurements also show that eventually the scale of the secondary structure increases. The mean position for this has not been precisely determined but both the concentration measurements and the time exposures indicate it to be near the end of the mixing transition. The streaky pattern is still seen on instantaneous pictures far downstream of the mixing transition (e.g., Konrad, 1976) and on high speed schlieren motion pictures which we obtained.

Downstream of the transition the pattern does not come through on time exposures because it varies from frame to frame, apparently with the scale of the primary vortices, which now have a broad distribution. The mean value of the spanwise spacing now scales with the local vorticity thickness, specifically $\lambda/\delta_\omega = 1.0$. (Jimenez et al. proposed $\lambda/\delta_\omega \sim 1$ to 1.25 on the basis of their spanwise measurements of the velocity field.) It is also interesting to compare this result with velocity correlation measurements at high Reynolds number by Browand and Troutt (1980) who found a large value of correlation coefficient (> 80%) for spanwise spacing smaller than δ_ω, dropping to 40% for $2.3\delta_\omega$. Degradation of the correlation is possibly related to the secondary vortex structure.

Finally we note an interesting connection with the observations, in Part I, of the growth of the primary vortices during their lifetimes, as seen in edge view. Much of that growth may be the result of the induced motions, away from the primary vortex cores, of the warped, secondary vortices.

Whether there is need for additional instabilities to account for the mixing transition is not clear. The secondary vortices themselves increase the interface considerably, as seen in the cross-sectional pictures. Furthermore, after the vorticity is increased by stretching along the braids and periphery of the cores, amalgamation of the primary vortices results in accumulation of that stretched vorticity into the newly formed core. Consequently, entrained but unmixed fluid in the spanwise vortex cores in the initial, two-dimensional region

will be mixed progressively after the appearance of the secondary vortex structure and a few amalgamations. Comparison of the mixing transition Reynolds number with that of the onset of the secondary structure indicates that (for $s = 7$ and $r = 0.38$) it encompasses, on average, 2.5 amalgamations by pairing.

Epilogue

The coherent structure of turbulent mixing layers has been investigated. The results of several experiments and theoretical developments dealing with the primary spanwise and the secondary streamwise vortex structures have been presented. It is hoped that these provide some further insights into the physical processes occurring in a turbulent mixing layer and will motivate additional research in this challenging field of Fluid Mechanics.

References

Aitchison, J. and Brown, J.A.C. (1957) The lognormal distribution Cambridge University Press.

Bradshaw P. (1966) "The effects of initial conditions on the development of a free shear layer" J. Fluid Mech. 26, 225-236.

Breidenthal, R.E. (1978) "A chemically reacting turbulent shear layer" Ph.D. Thesis, California Institute of Technology.

Browand, F.K. and Troutt, T.R. (1980) "A note on spanwise structure in the two-dimensional mixing layer" J. Fluid Mech. 97, 771-781

Brown, G.L. (1974) "The entrainment and large structure in turbulent mixing layers" Proc. 5th Australasian Conference on Hydraulics and Fluid Mechanics, 352-359.

Brown, G.L. and Rebollo, M.R. (1972) "A small, fast-response probe to measure composition of a binary gas mixture" AIAA Journal 10, 649-652.

Brown, G.L. and Roshko, A. (1971) "The effect of density difference on the turbulent mixing layer" AGARD-CP-93, 23-1 to 23-11.

Brown, G.L. and Roshko, A. (1974) "On density effects and large structure in turbulent mixing layers" J. Fluid Mech. 64, 775-816.

Corcos, G.M. (1979) "The mixing layer: deterministic models of a turbulent flow" U.C. Berkeley Report No. FM-79-2.

Dewey, C.F., Jr. (1976) "Qualitative and quantitative flow field visualization utilizing laser-induced fluorescence" AGARD-CP-193, 17-1 to 17-7.

Dimotakis, P.E. and Brown, G.L. (1976) "The mixing layer at high Reynolds number: Large-structure dynamics and entrainment" J. Fluid Mech. 78, 535-560.

Hernan, M.A. and Jimenez, J. (1979) "The use of digital image analysis in optical flow measurements" Proc. 2nd Symp. on Turbulent Shear Flows, Imperial College, London, July 2-4.

Ho, C. -M. and Huang, L.S. (1980) "Subharmonics and vortex merging in mixing layers" Submitted to J. Fluid Mech.

Hussain, A.K.M.F. and Zeda, M.F. (1978) "Effects of the initial condition on the axisymmetric free shear layer: effects of the initial momentum thickness" Phys. of Fluids 21, 1100-1112.

Jimenez, J., Martinez-Val, R. and Rebollo, M. (1979) "On the origin and evolution of three-dimensional effects in the mixing layer" Final Technical Report, Grant Number DA-ERO 78-G-079.

Kolpin, M.A. (1964) "The flow in the mixing region of a jet" J. Fluid Mech. 18, 529-548.

Konrad, J.H. (1976) "An experimental investigation of mixing in two-dimensional turbulent shear flows with applications to diffusion-limited chemical reactions" Ph.D. Thesis, California Institute of Technology, also Project SQUID Technical Report CIT-8-PU.

Koochesfahani, M.M., Catherasoo, C.J., Dimotakis, P.E., Gharib, M. and Lang, D.B. (1979) "Two-point LDV measurements in a plane mixing layer" AIAA Journal 17, 1347-1351.

Moore, D.W. and Saffman, P.G. (1972) "Structure of a line vortex in an imposed strain" in Aircraft Wake Turbulence and its Detection (Olson, John H. et al., eds.) Plenum Press, 339-354.

Moore, D.W. and Saffman, P.G. (1975) "The density of organized vortices in a turbulent mixing layer" J. Fluid Mech. 69, 465-473.

Patnaik, P.C., Sherman, F.S. and Corcos, G.M. (1976) "A numerical simulation of Kelvin-Helmholtz waves of finite amplitude" J. Fluid Mech. 73, 215-240.

Pierrehumbert, R.T. (1980) "The structure and stability of large vortices in an inviscid flow" Ph.D. Thesis, Massachusetts Institute of Technology.

Roshko, A. (1976) "Structure of turbulent shear flows; a new look" AIAA Journal 14, 1349-1357.

Takaki, R. and Kovasznay, L.S.G. (1978) "Statistical theory of vortex merger in the two-dimensional mixing layer" Phys. of Fluids 21, 153-156.

Toor, H.L. (1962) "Mass transfer in dilute turbulent and non-turbulent systems with rapid irreversible reactions and equal diffusivities" A.I.Ch.E. Journal 8, 70-78.

Winant, C.D. and Browand, F.K. (1974) "Vortex pairing: the mechanism of turbulent mixing layer growth at moderate Reynolds number" J. Fluid Mech. 63, 237-255.

	R_{θ_1}	x_t/θ_1	$-x_0/\theta_1$
Bradshaw (1966)		1000	
Breidenthal (1978)	200	800	
Hussain and Zedan (1978)	349	250	35
	204	310	110
	185	600-400	214-150
Large Scale Self-similarity	180	560	200

Table I.1 Summary transition data for constant density mixing layers with initial laminar boundary layers.

	$k_A = I(\sigma)$	σ	$\overline{\zeta}_F/\overline{\zeta}$	$\overline{\zeta}_A/\overline{\zeta}$	$\overline{L}/X$
Tearing	3	.1617	.7975	1.1983	.4017
Pairing	2	.2760	.6602	1.3301	.6731
Tripling	3/2	.4363	.4840	1.4947	1.0216

Table I.2 Summary of theoretical results.

P_0 (atm)	L_{BL} (cm)	r	$\Delta U/U_c$	U_1 (cm/s)	$\frac{\Delta U \delta_{v_0}}{\nu_{N_2}} \times 10^{-3}$	$\frac{\bar{\lambda}_{3D}}{\lambda_{2Di}}$	$\frac{\bar{\lambda}_{3D}}{\lambda_{2D_0}}$	$\frac{\lambda'_{3D}}{\lambda_{2D_0}}$
4	3.0	.15	2.16	1467 992	13.3 14.8	1.63 1.25	.93 .68	.20 .16
		.3	1.39	1470 998 752	10.1 10.7 9.6	1.31 1.21 1.22	.70 .67 .56	.28 .16 .08
		.38	1.10	1008 740 504	6.1 6.3 6.7	1.29 1.29 1.20	.68 .51 .65	.27 .21 .05
		.5	.77	1012 755 496	3.3 3.3 3.1	1.17 1.50 1.42	.78 .75 .64	.30 .27 .09
6	3.0	.38	1.10	1000 651	5.7 7.0	1.40 1.25	.70 .56	.26 .23
4	5.5	.38	1.10	996 758	9.5 9.4	1.47 1.20	.67 .66	.17 .12

Table II.1 Summary of Three Dimensional Instability Data for s = 7.

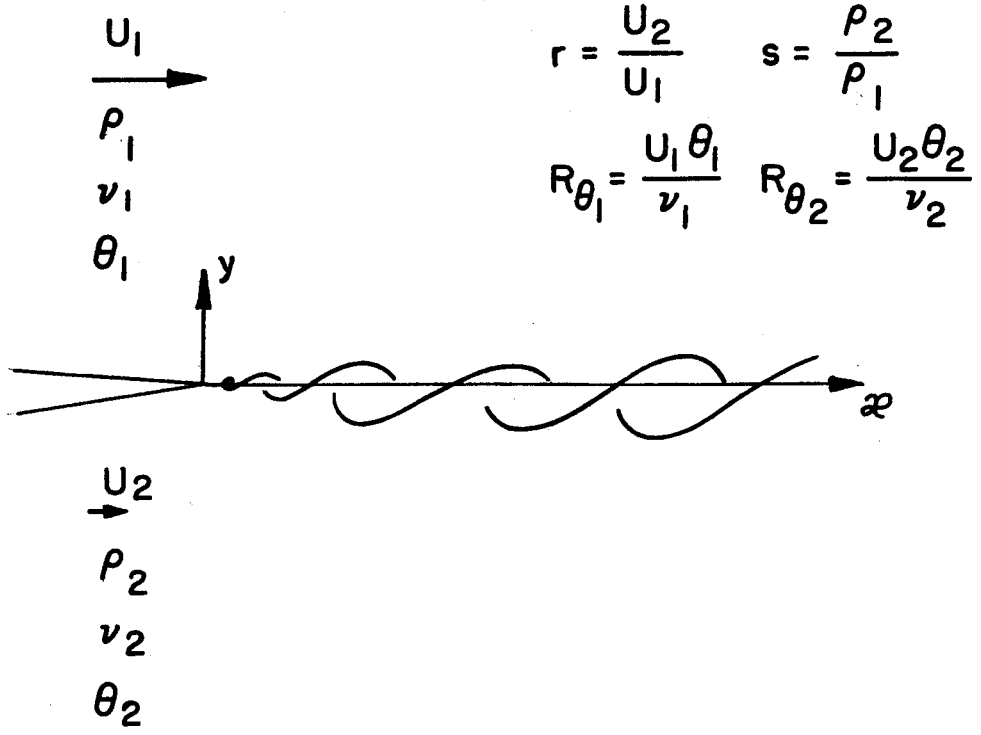

Figure I.1 Mixing layer parameters and coordinate system.

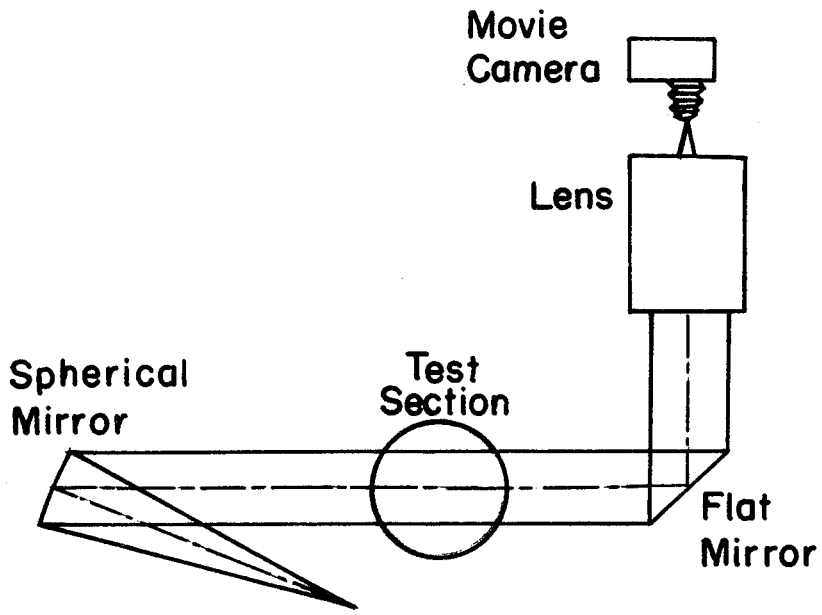

Figure I.2 Shadowgraph optical system.

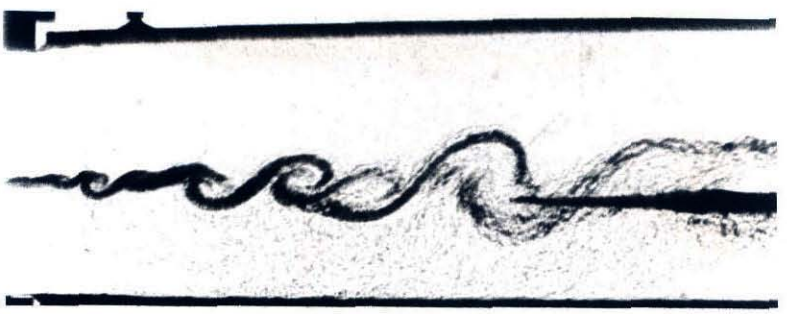

Figure I.3 Shadowgraph picture. U_1 = 1000 cm/s, r = 0.38, s = 1, p_0 = 8 atm.

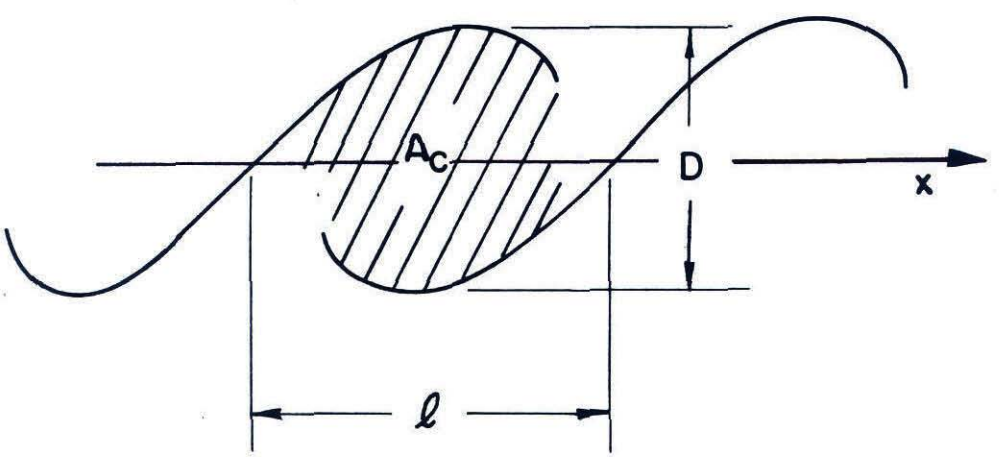

Figure I.4 Visual properties of large scale vortices measured; ℓ circulation, D visual thickness, A_c area of the core.

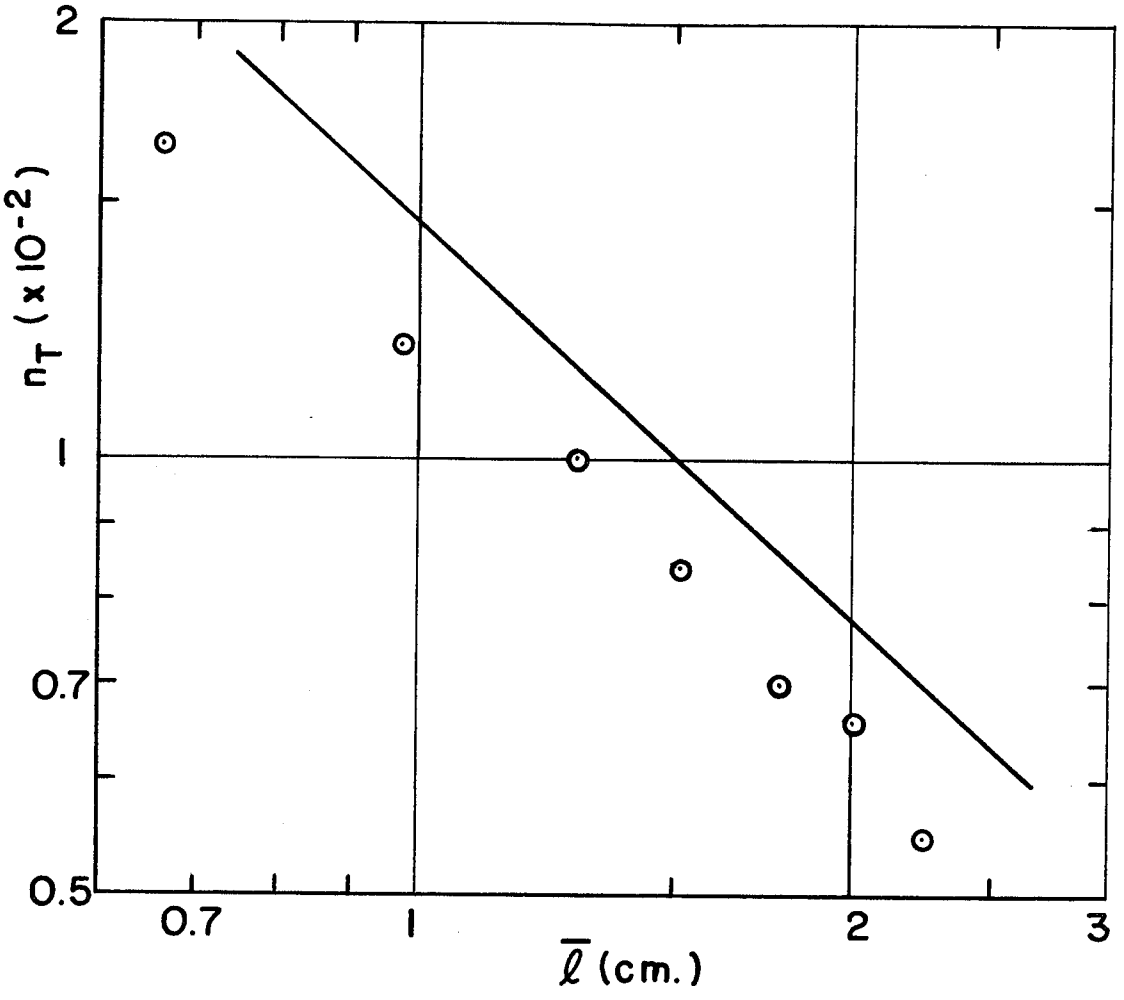

Figure I.5 Sample size as a function of mean circulation; (——) $n_T = U_c \tau_s / \bar{\ell}$, ⊙ measurements.

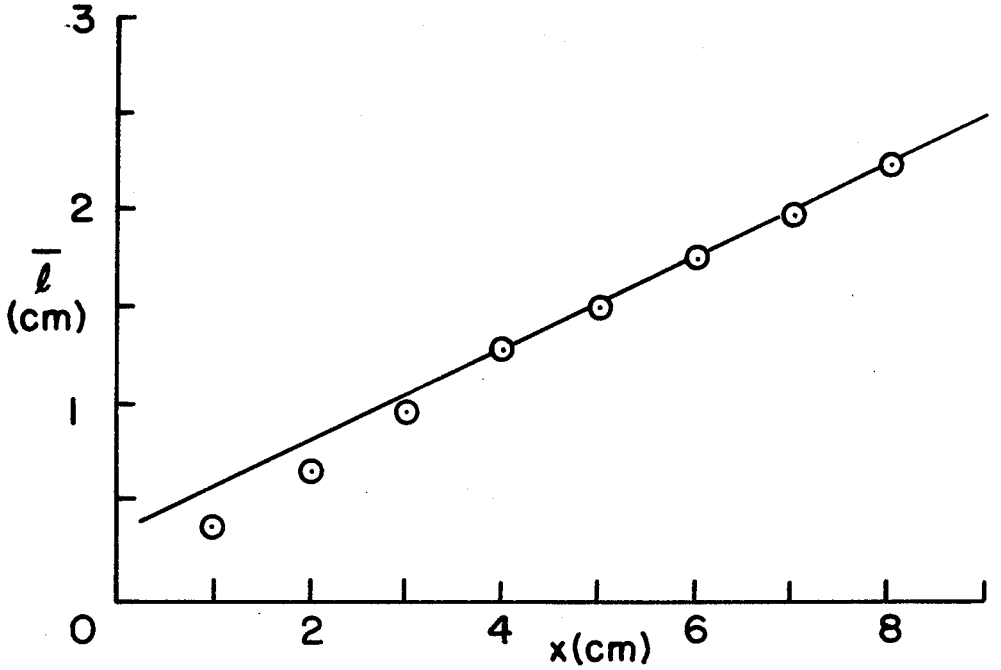

Figure I.6 Mean circulation as a function of downstream position. (——), least squared fit to measured points with $x \geq 4$ cm.

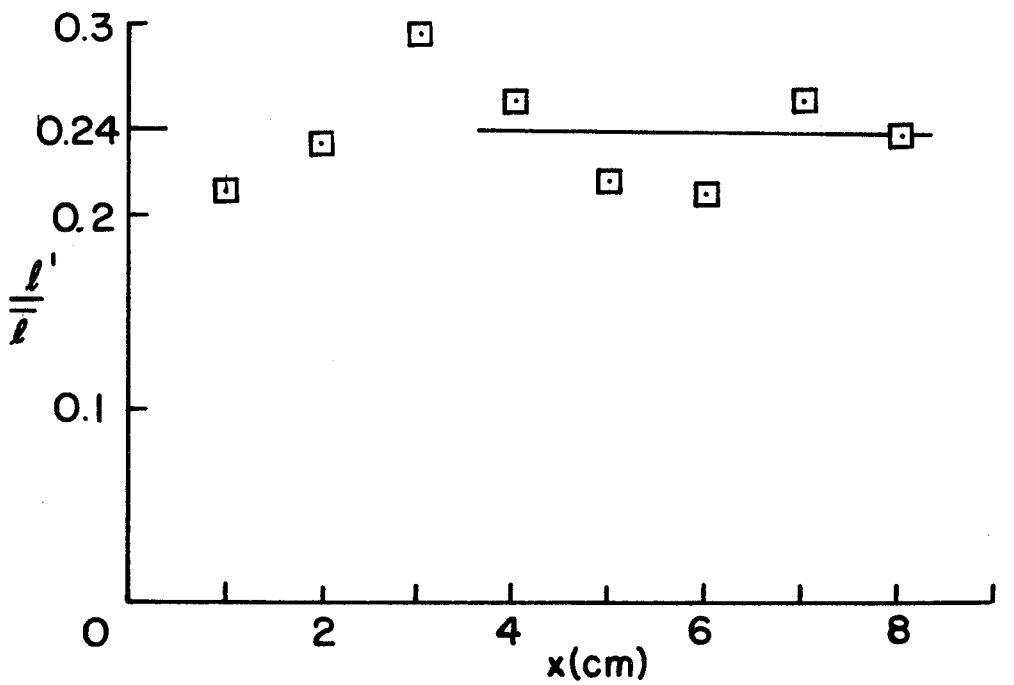

Figure I.7 Normalized rms deviation of the circulation as a function of downstream position. (——), average value $x \geq 4$ cm.

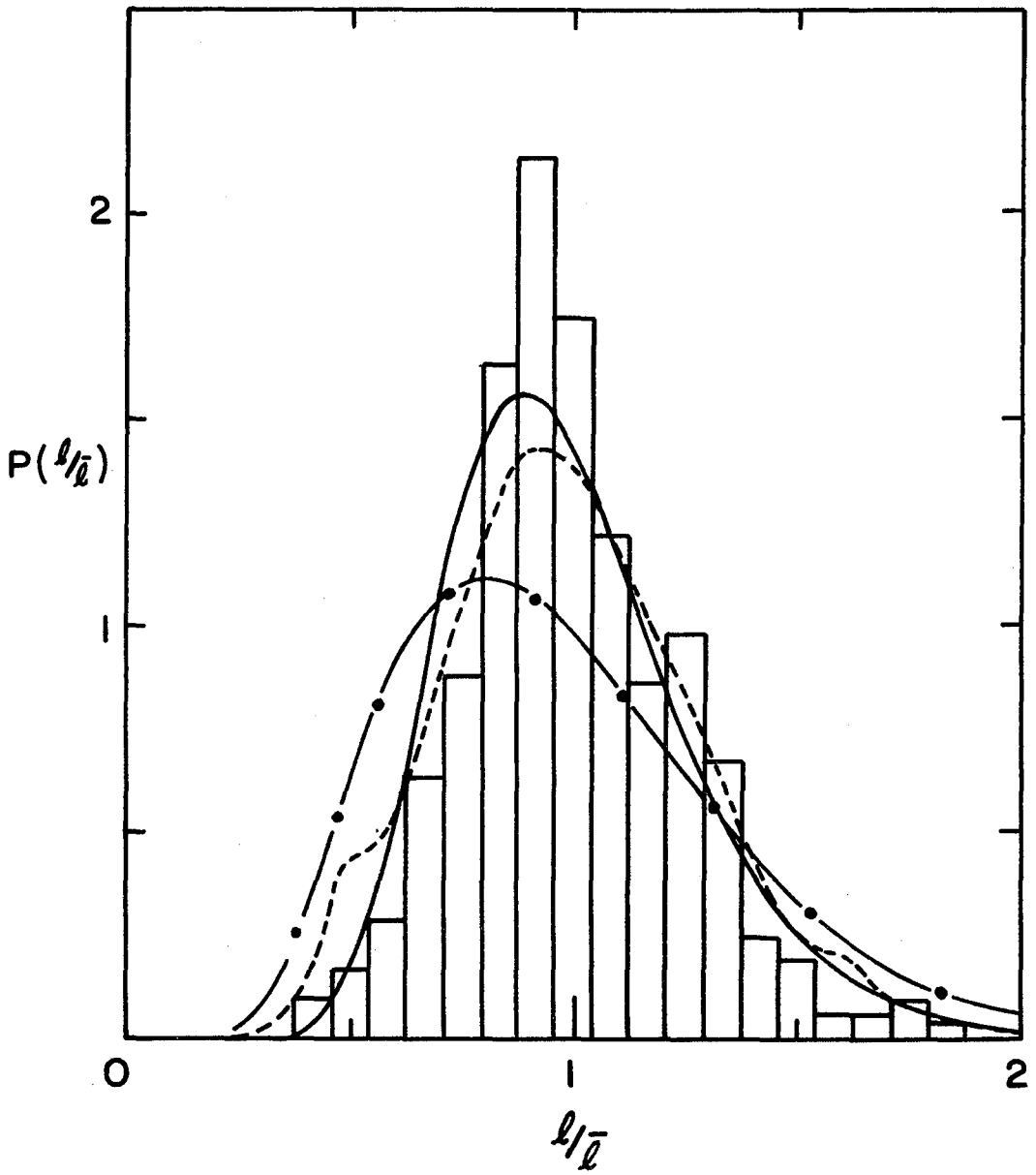

Figure I.8 Vortex circulation probability distribution. Histogram present measurements; (- - -), Brown and Roshko (1974); (- • -), Takaki and Kovasznay (1978); (——), Theory chapter I.3.

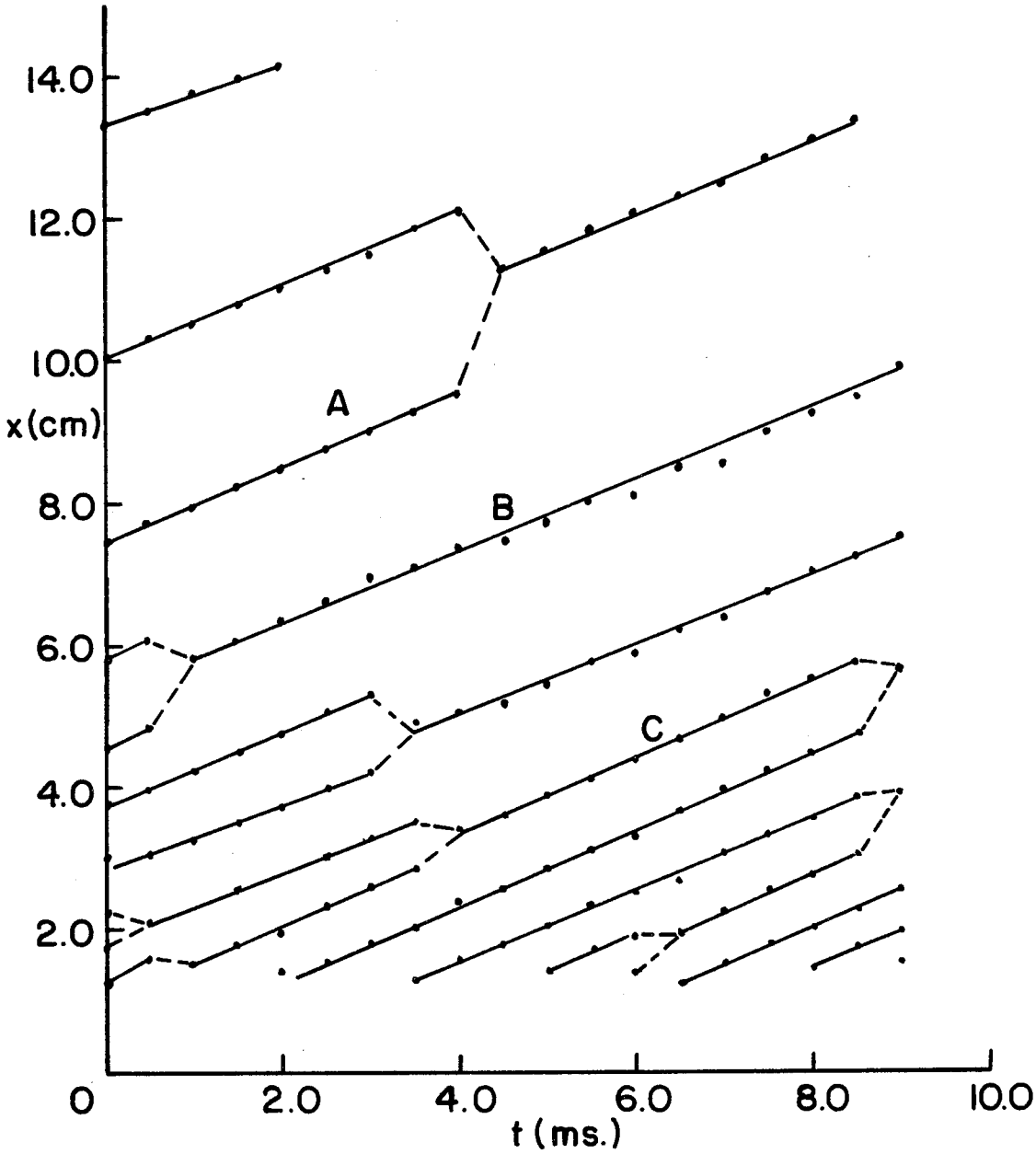

Figure I.9 x-t diagram of vortices used in mean evolution evaluation. Vortex histories A, B, and C are those used for comparison in following figures.

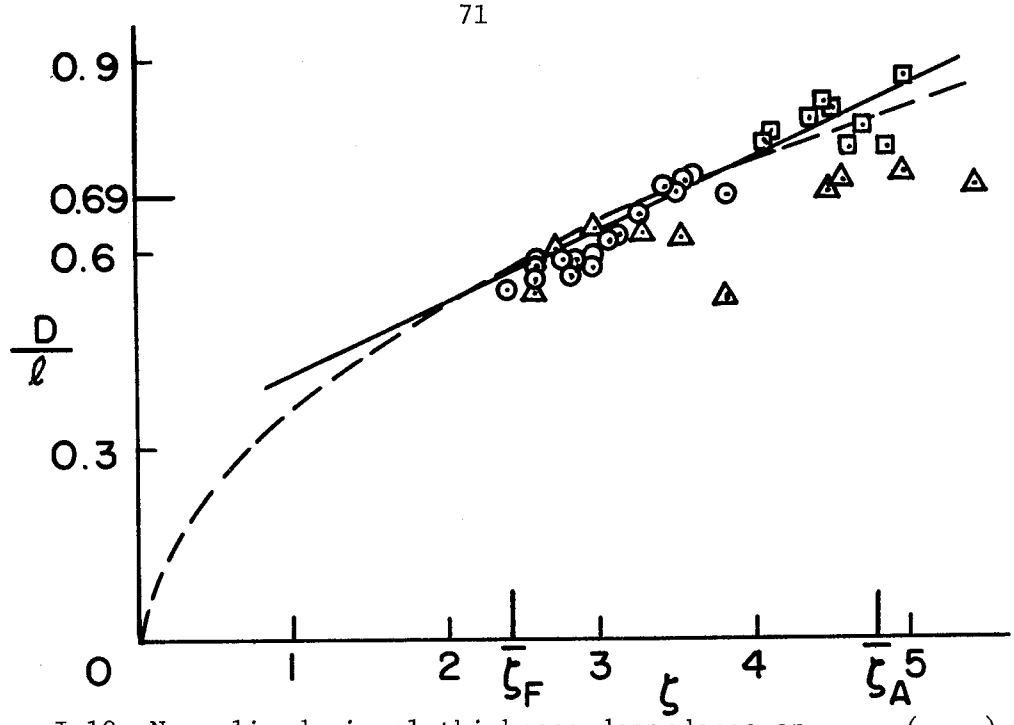

Figure I.10 Normalized visual thickness dependence on ζ. (——), $D/\ell = 0.11\zeta + 0.31$; (- -), $D/\ell = 0.37\zeta^{1/2}$; ⊡, Vortex A; ⊙, Vortex B; △, Vortex C. $\overline{\zeta}_F = 2.4$, $\overline{\zeta}_A = 3.6$, $\overline{D/\ell} = 0.69$.

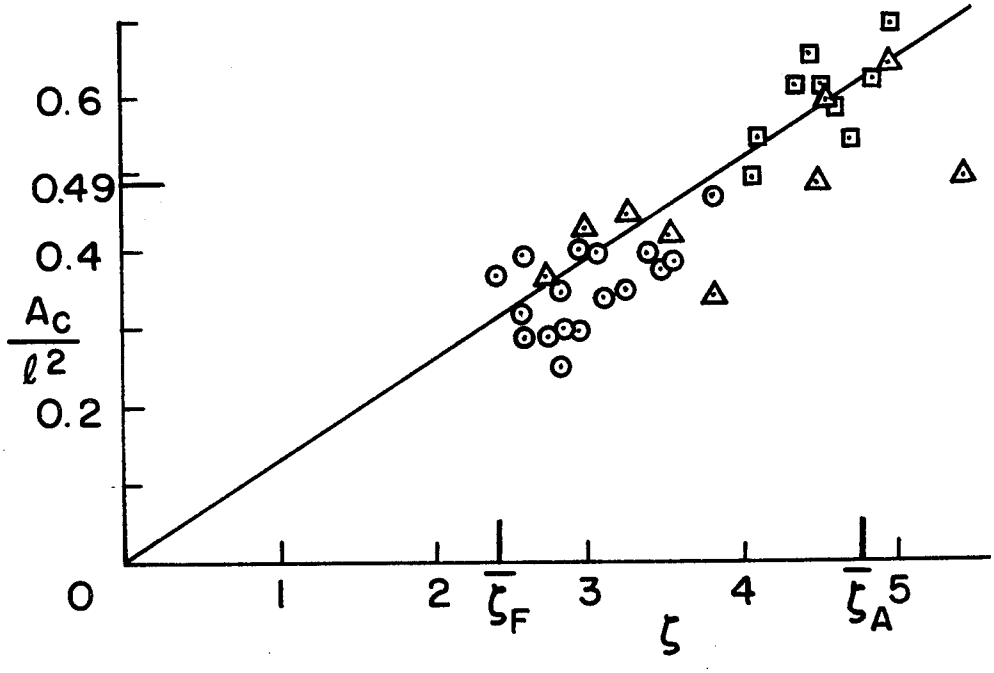

Figure I.11 Normalized core area dependence on ζ. (——), Mean evolution; ⊡, Vortex A; ⊙, Vortex B; △, Vortex C. $\overline{\zeta}_F = 2.4$, $\overline{\zeta}_A = 3.6$, $\overline{A_c/\ell^2} = 0.49$.

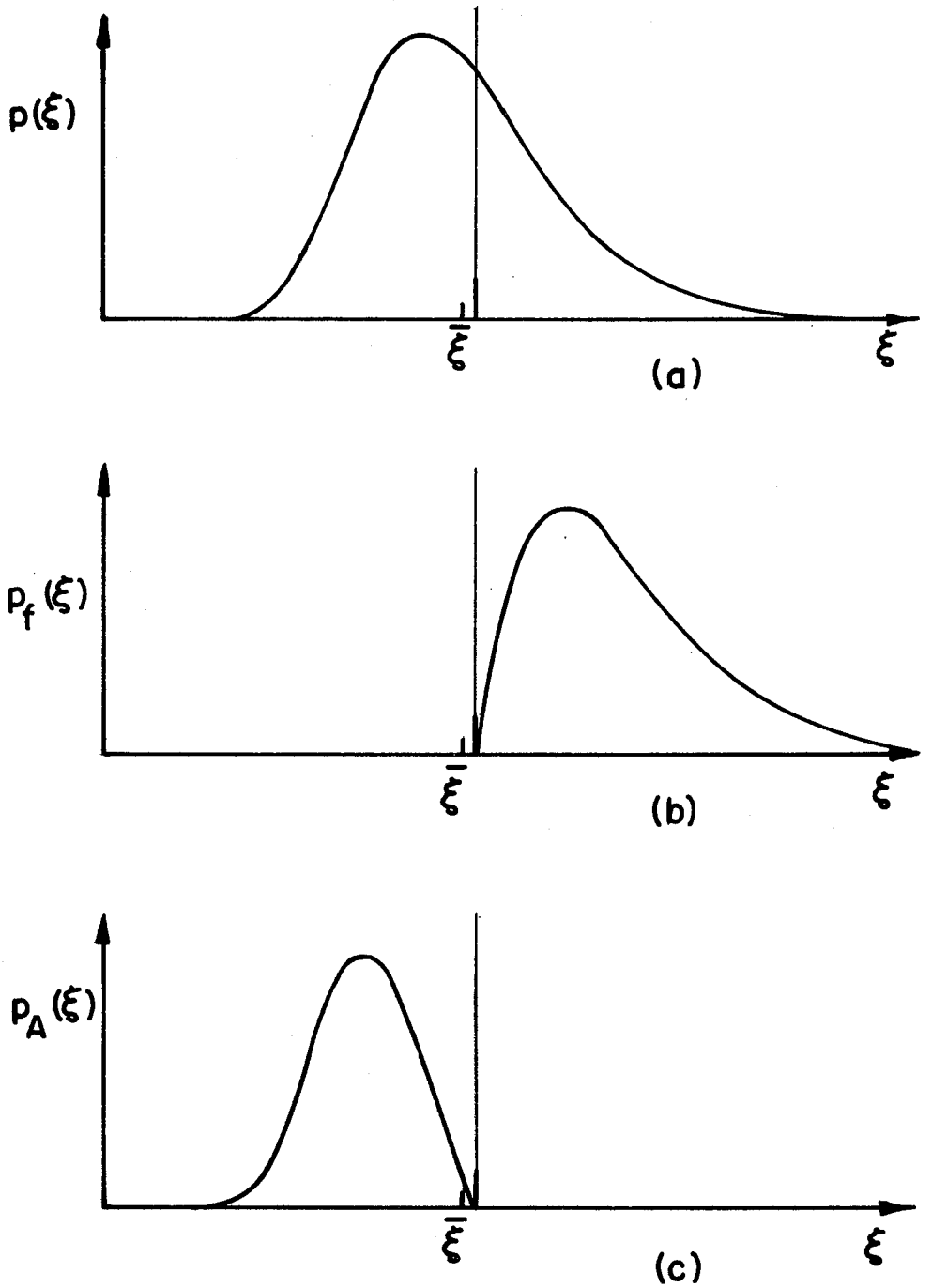

Figure I.12 Eulerian description (x fixed): (a) Vortex circulation probability distribution $p(\xi)$ (Eq. I.3.14); (b) Vortex formation probability distribution $p_F(\xi)$ (Eq. I.3.16); (c) Vortex annihilation probability distribution $p_A(\xi)$ (Eq. I.3.16).

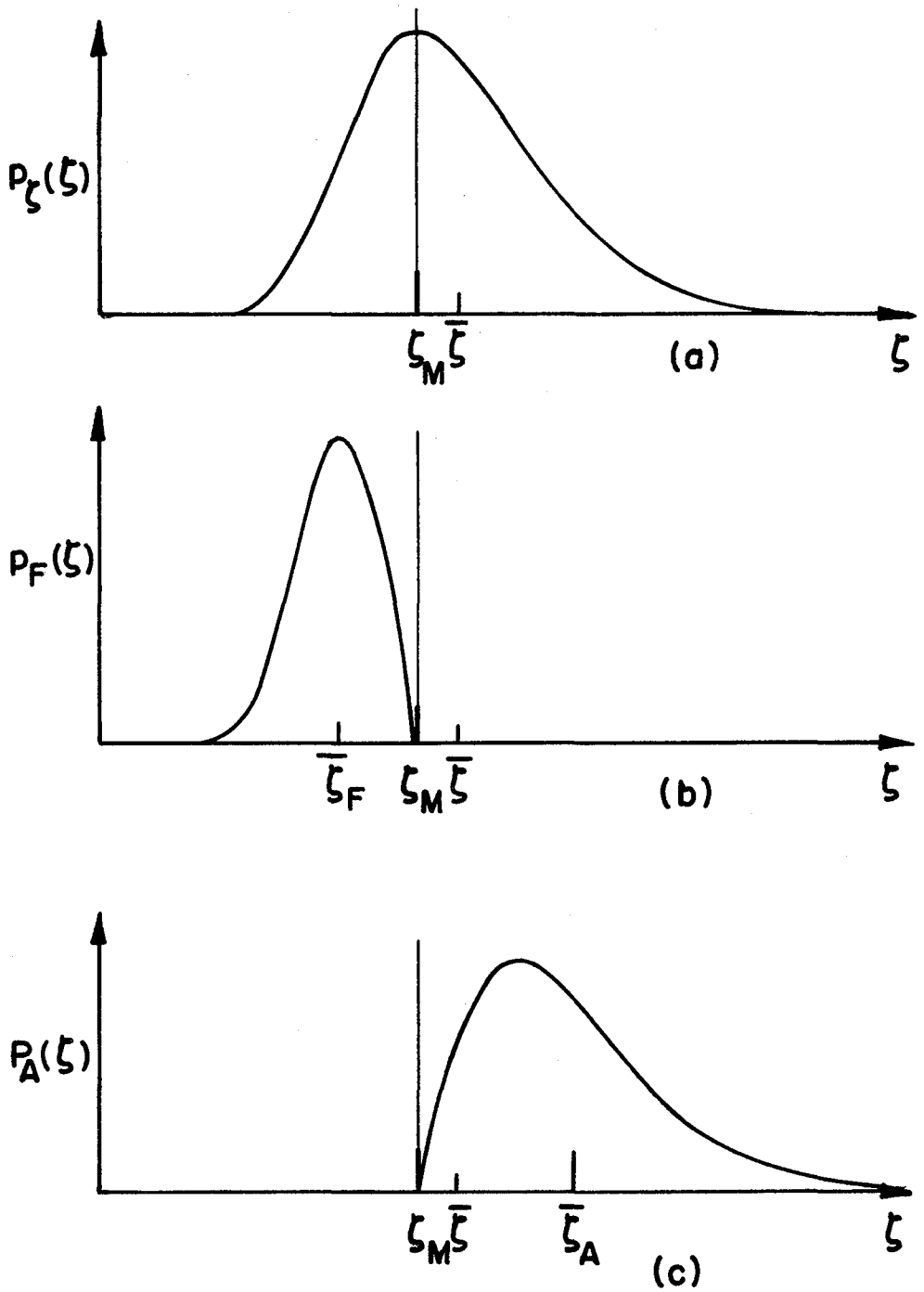

Figure I.13 Lagrangian description (ℓ fixed): (a) Vortex position probability distribution $p_\zeta(\zeta)$ (Eq. I.3.19); (b) Vortex formation probability distribution $p_F(\zeta)$ (Eq. I.3.20); (c) Vortex annihilation probability distribution $p_A(\zeta)$ (Eq. I.3.20).

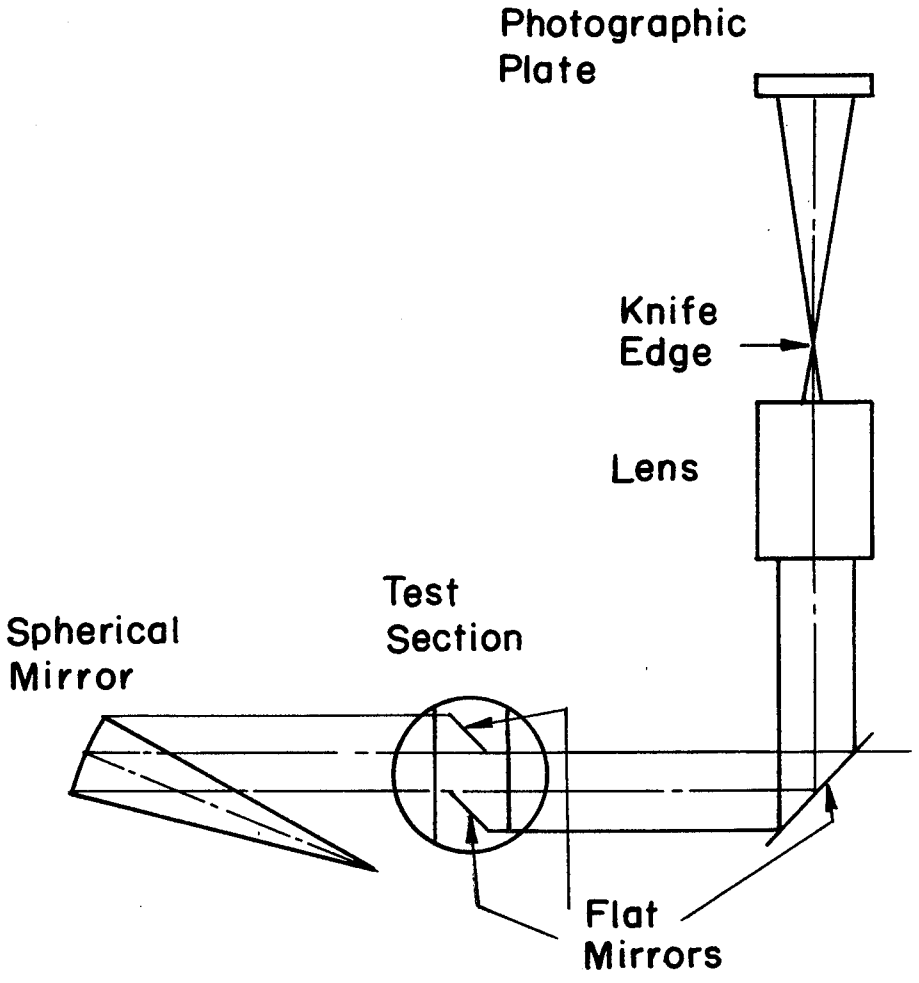

Figure II.1 Schlieren optical system.

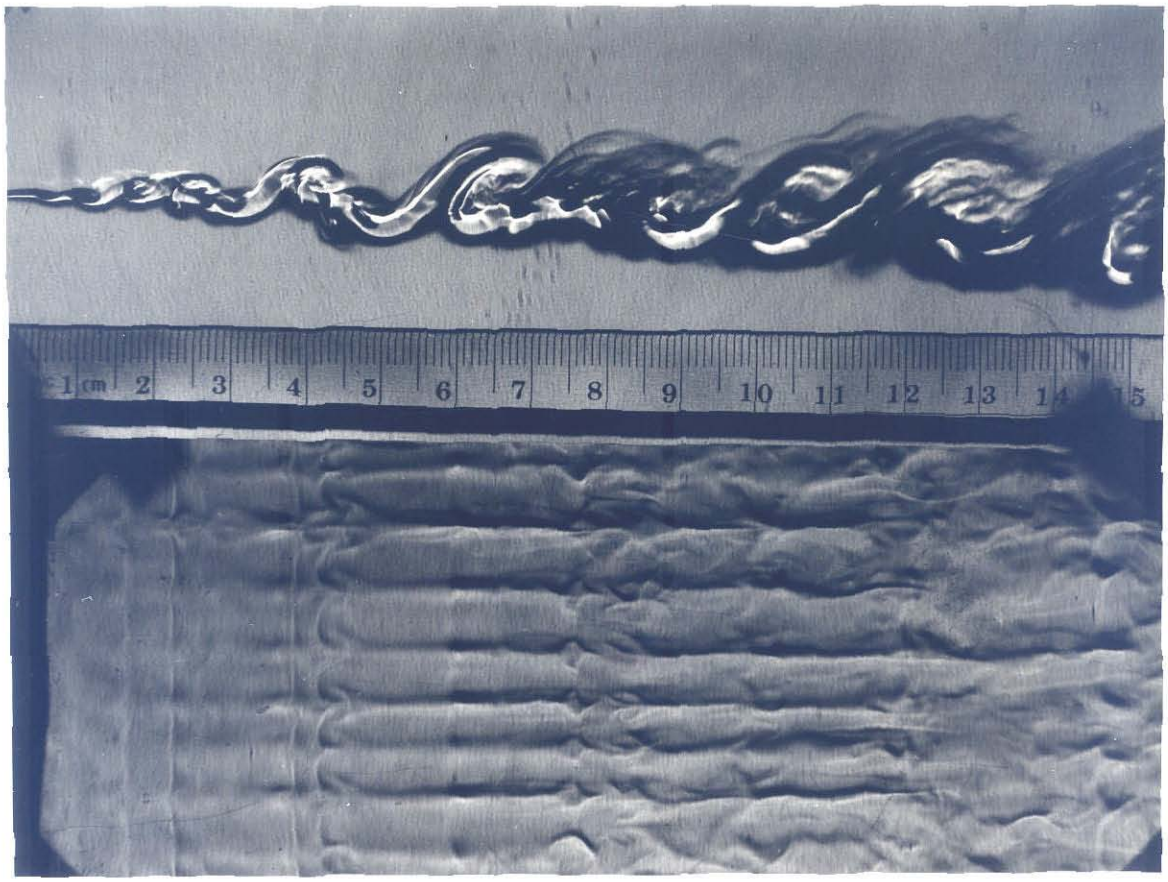

(a)

Figure II.2 Schlieren pictures of the helium-nitrogen mixing layer. Side view upper half, plan view lower half. U_1 = 496 cm/s, r = 0.5, s = 7, p_0 = 4 atm.

(a) 1 μs exposure.

(b) 2 second exposure.

(b)

Figure II.2 See legend on page 75

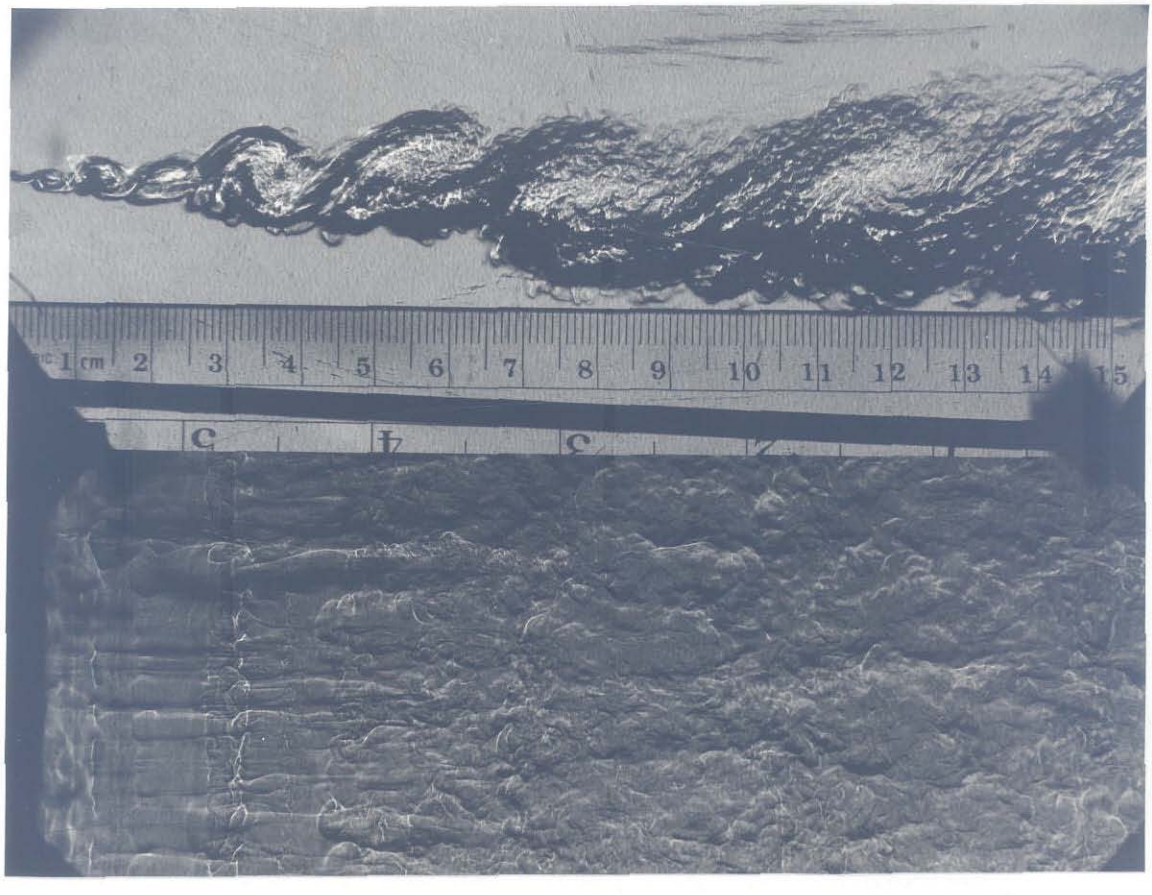

(a)

Figure II.3 Same as figure II.2 at conditions U_1 = 1470 cm/s, r = 0.3, s = 7, p_0 = 4 atm.
(a) 1 μs exposure.
(b) 2 second exposure.

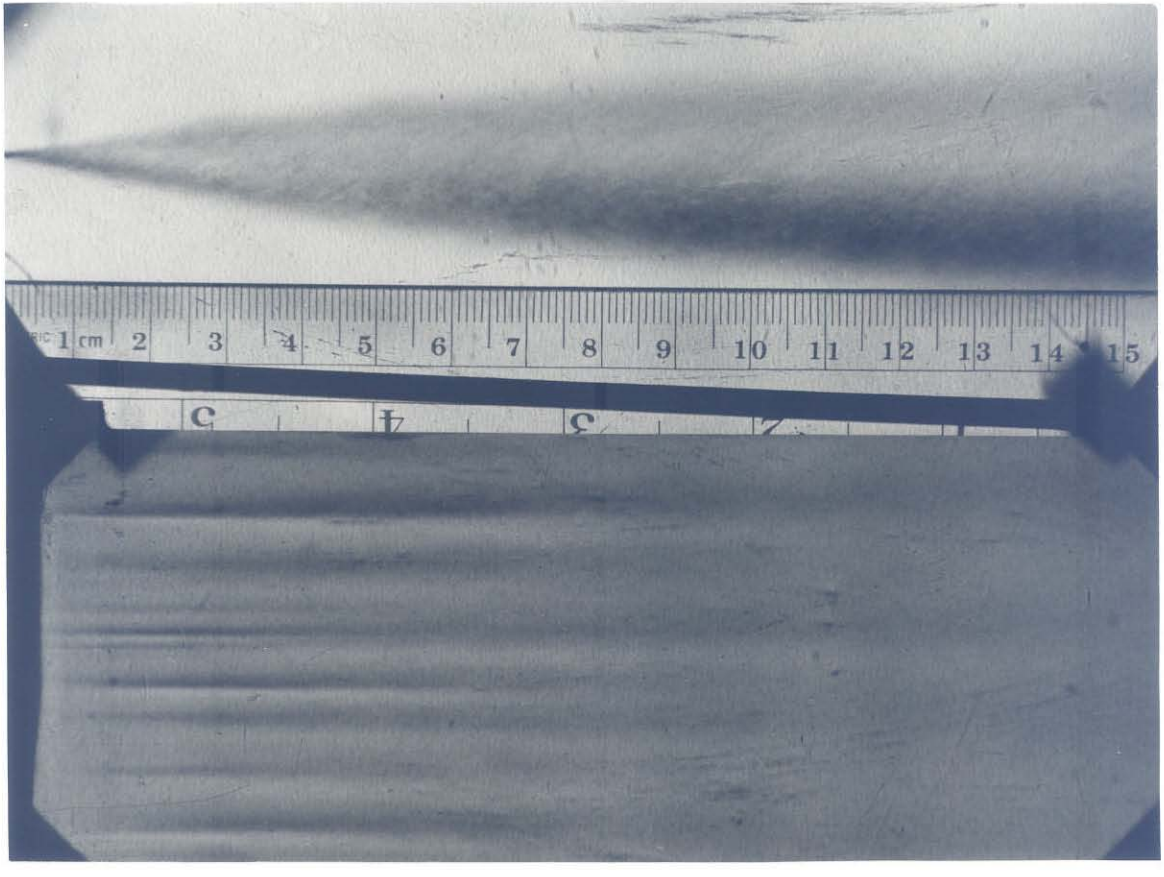

(b)

Figure II.3 See legend on page 77

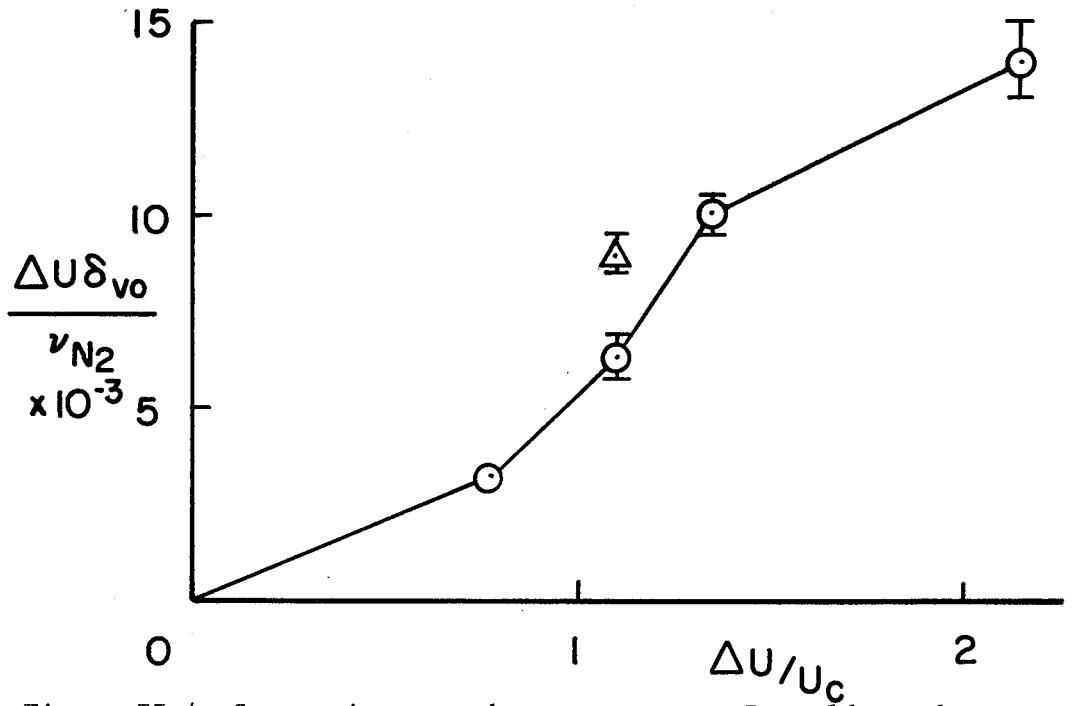

Figure II.4 Streamwise streak pattern onset Reynolds number as a function of $\Delta U/U_c$, s = 7. ⊙ Normal partition; △ Extended partition.

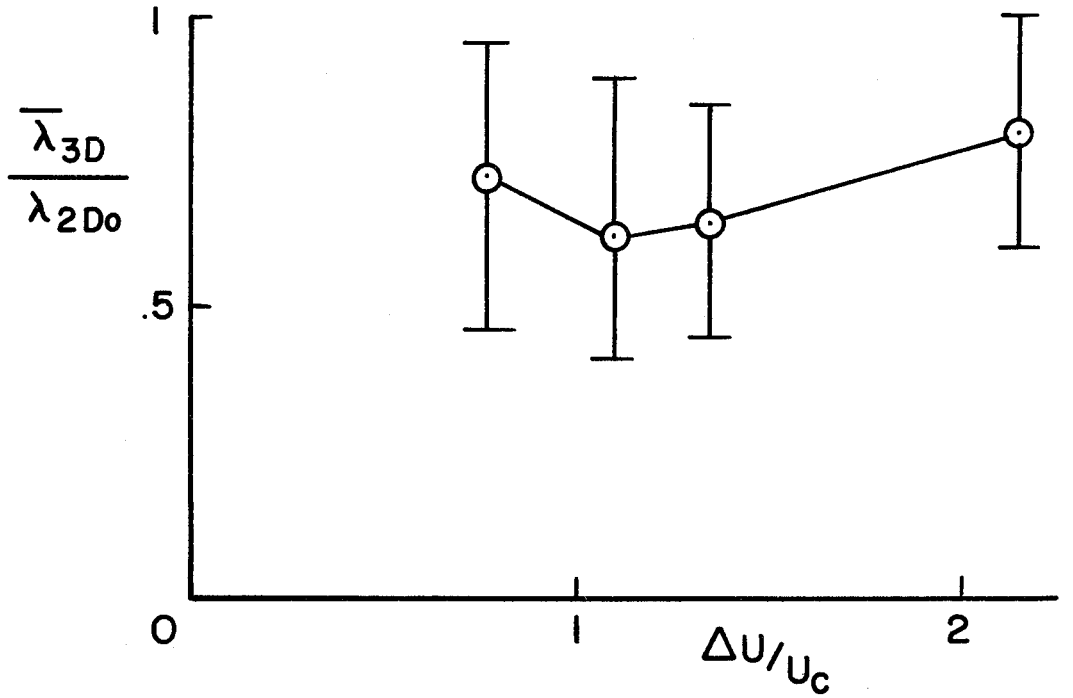

Figure II.5 Normalized streak spacing as a function of $\Delta U/U_c$, s = 7.

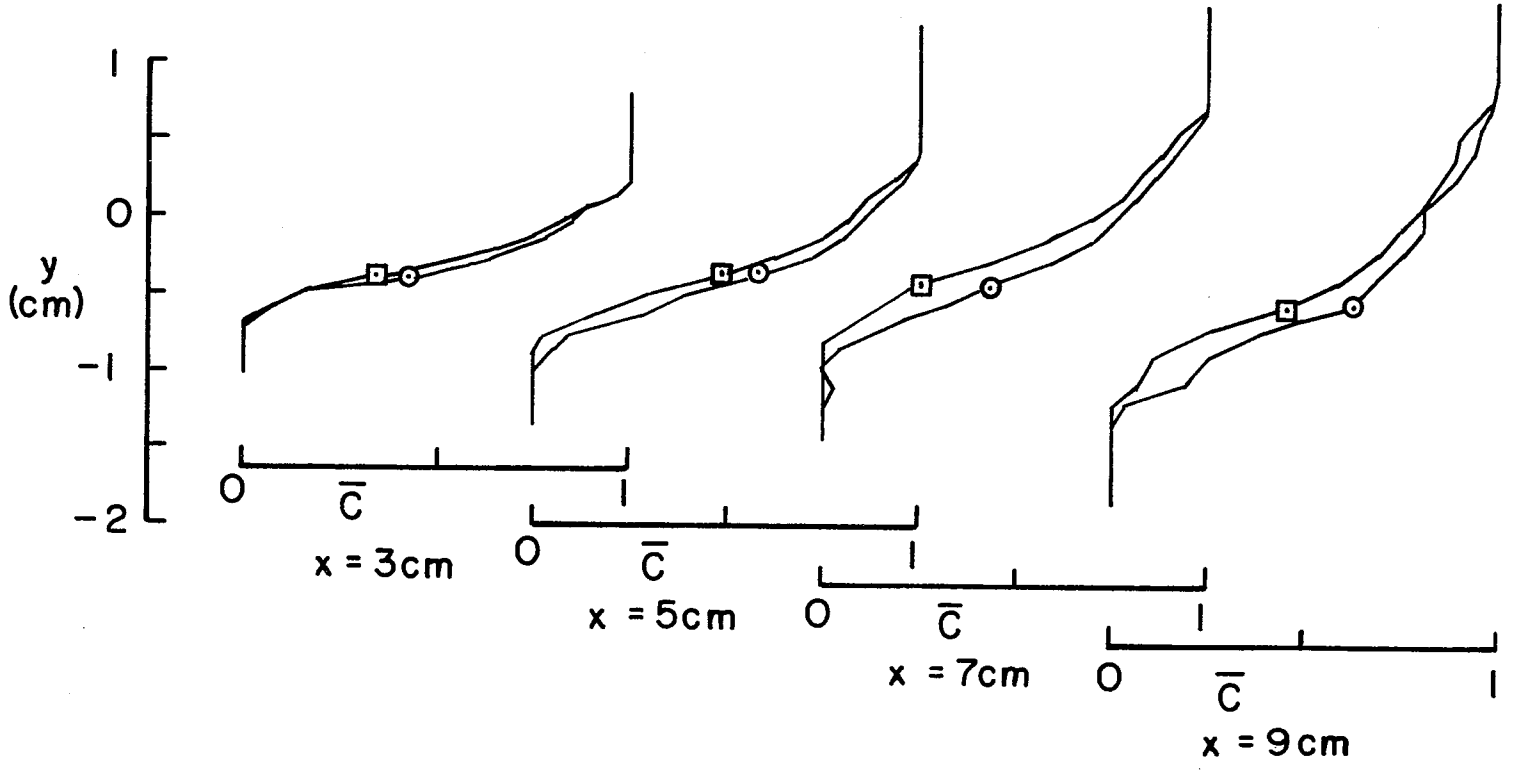

Figure II.6 Streamwise evolution of mean concentration profiles at two spanwise positions: ⊙ , z = 0; ⊡ , z = 0.64 cm. (Measured points in the profile are connected by straight line segments.)

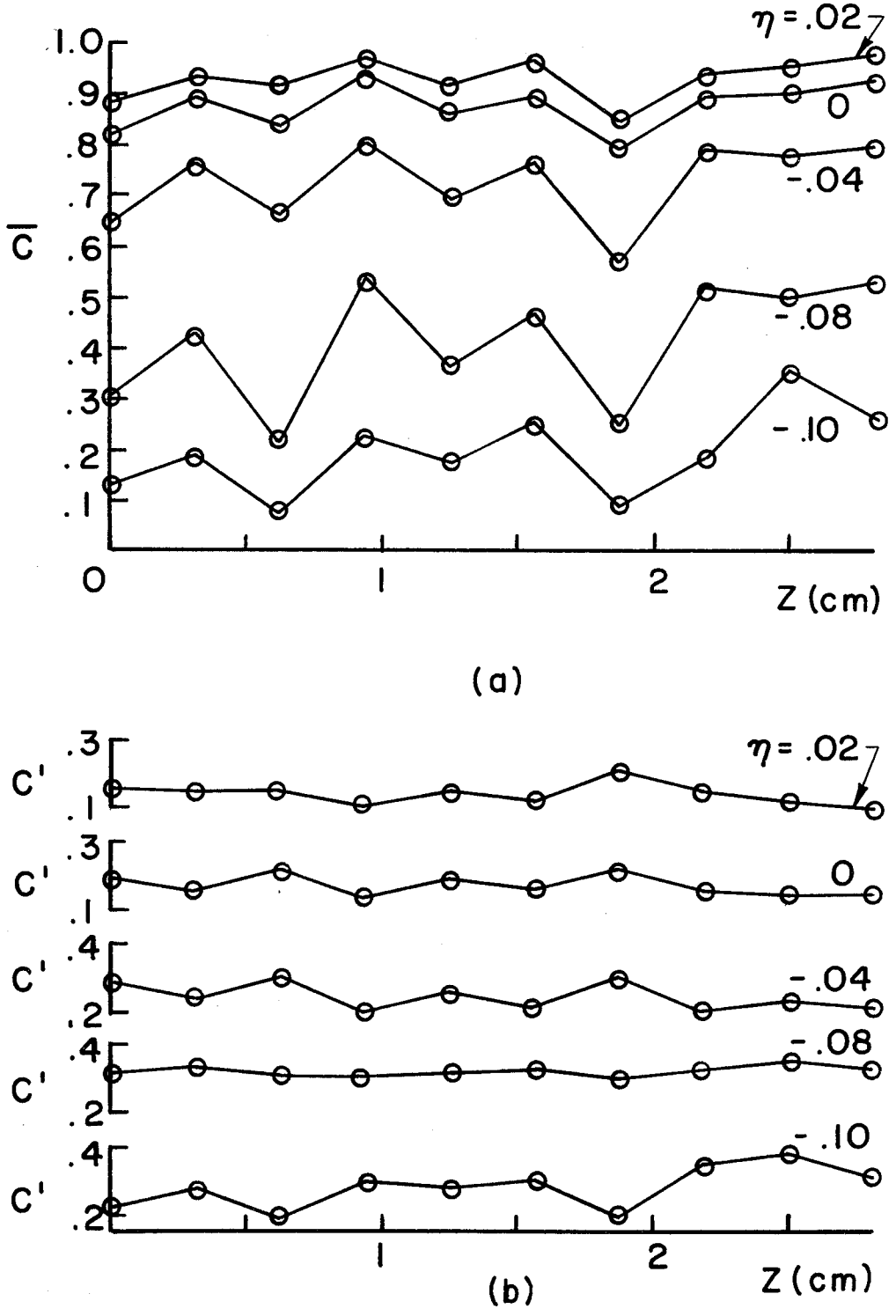

Figure II.7 Spanwise variation of the mean concentration (a) and its rms fluctuation (b) at various locations in the profile at x = 4 cm.

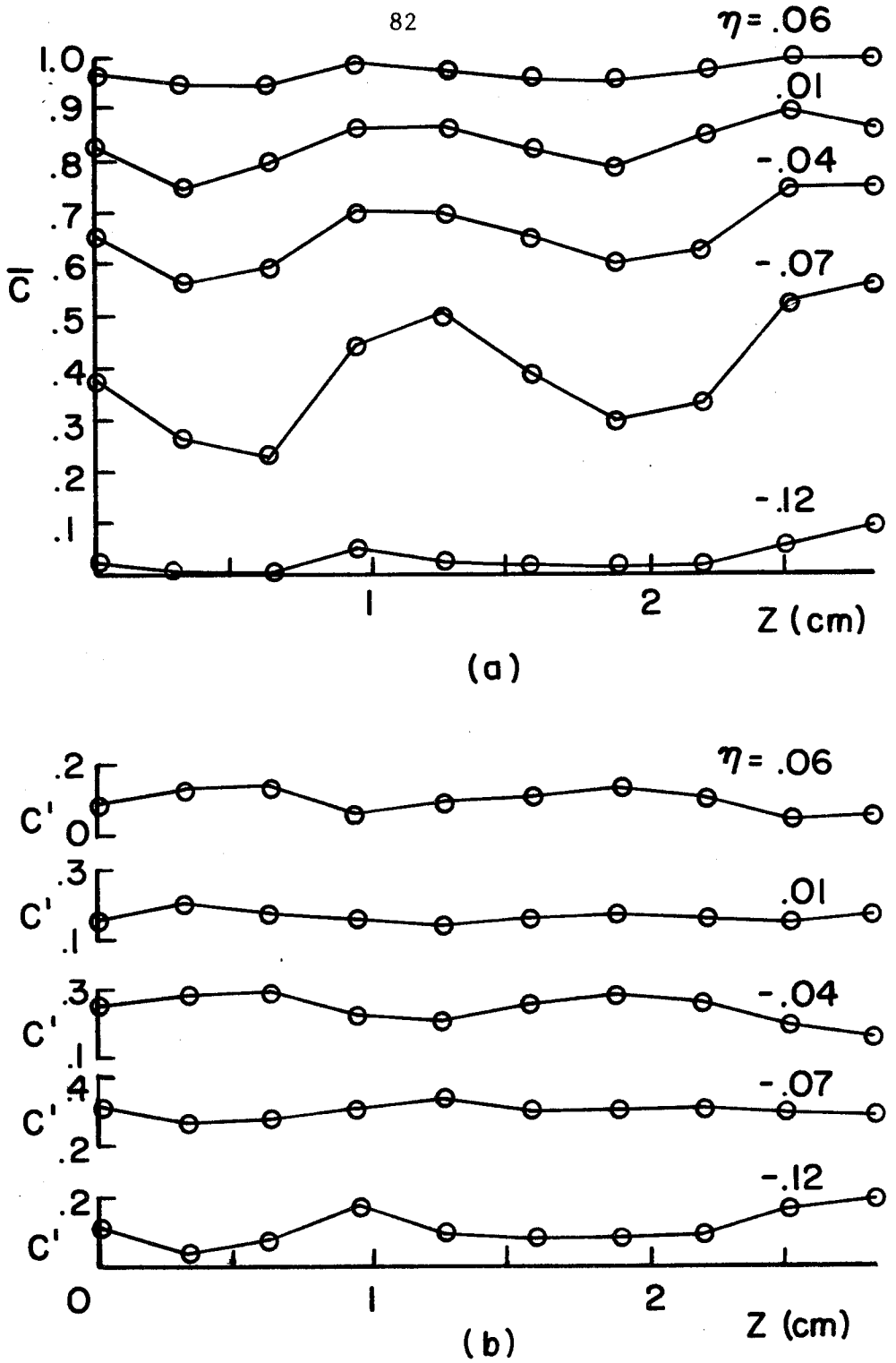

Figure II.8 Spanwise variation of the mean concentration (a) and its rms fluctuation (b) at various locations in the profile at x = 9 cm.

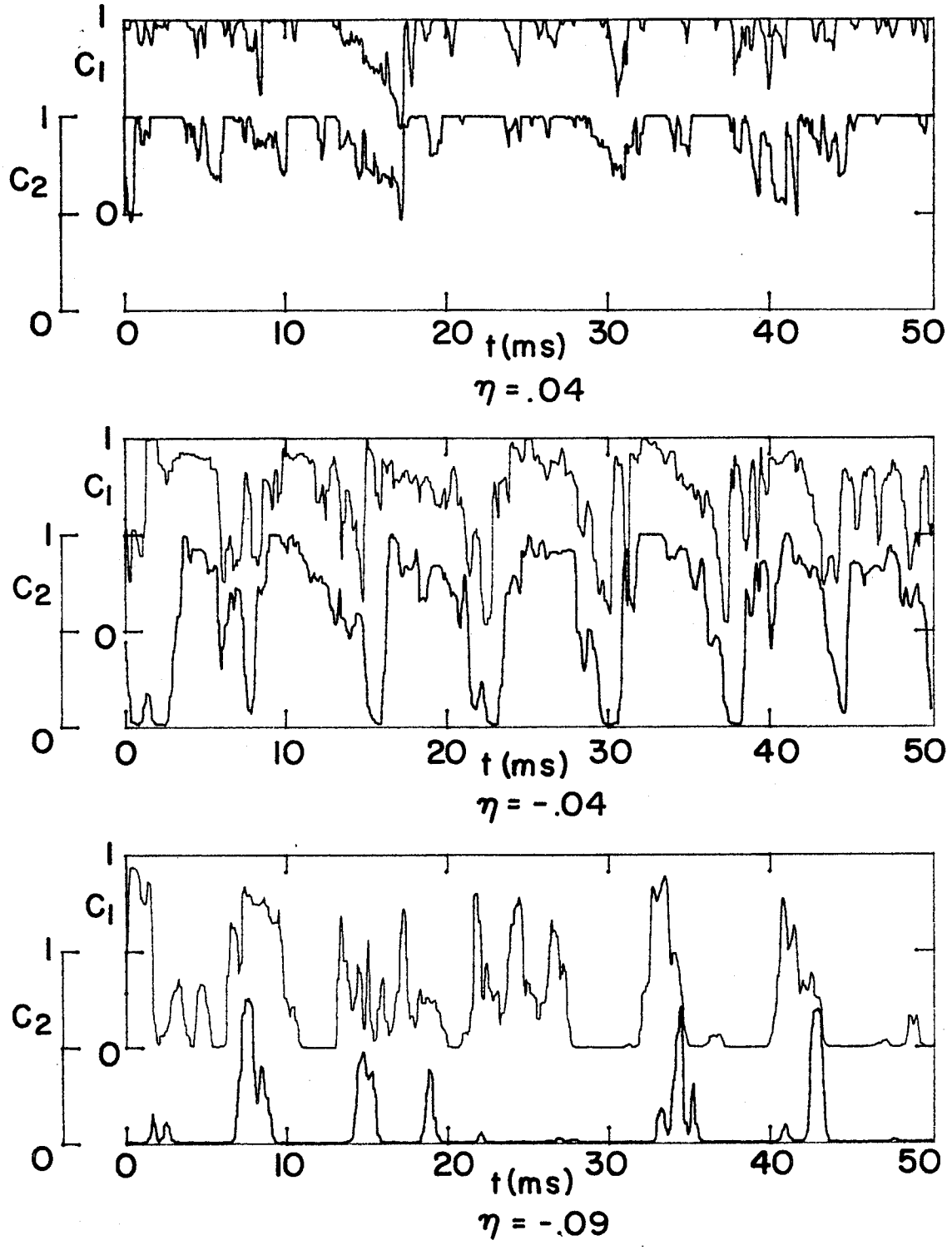

Figure II.9 Comparison of the concentration time histories at $z = 0$, C_1, and $z = 0.64$ cm, C_2, at $x = 9$ cm and three locations in the profile.

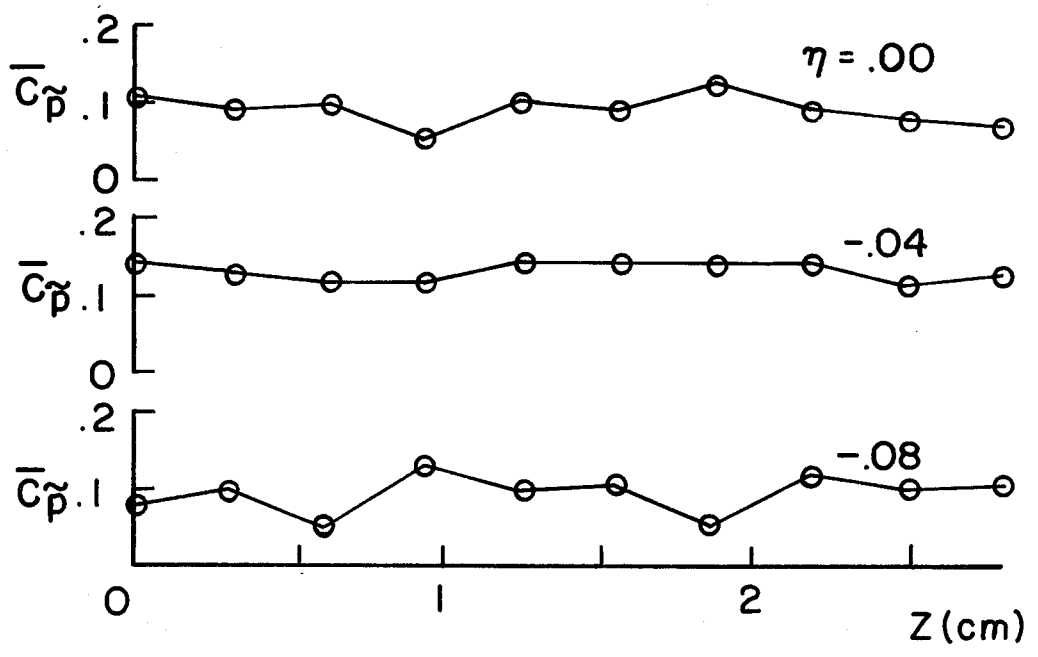

(a)

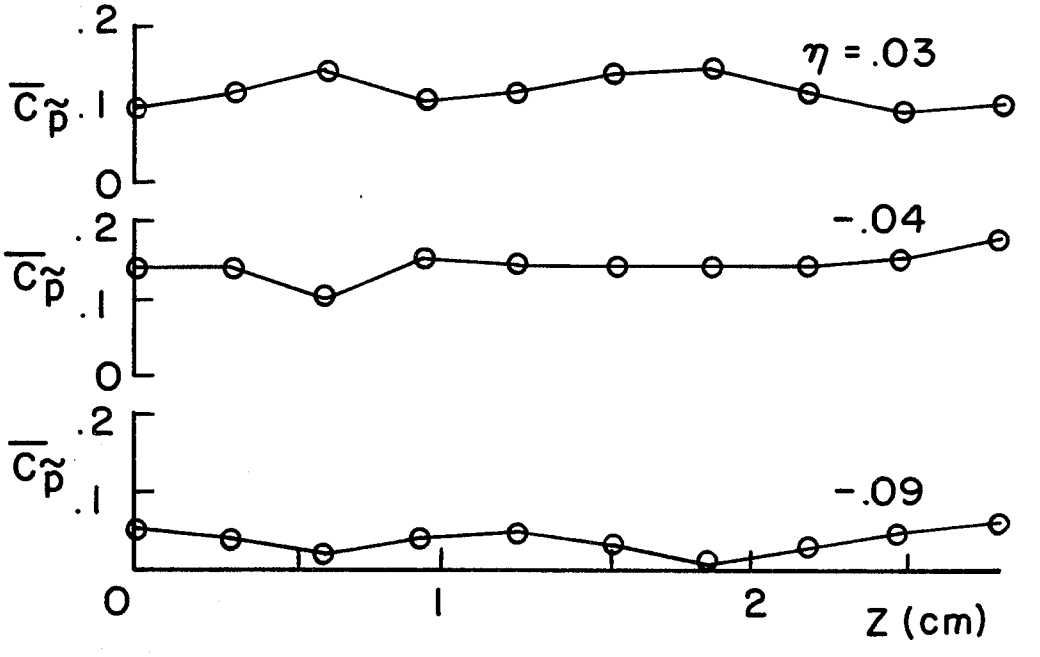

(b)

Figure II.10 Spanwise variation of mean product.
(a) x = 4 cm.
(b) x = 9 cm.

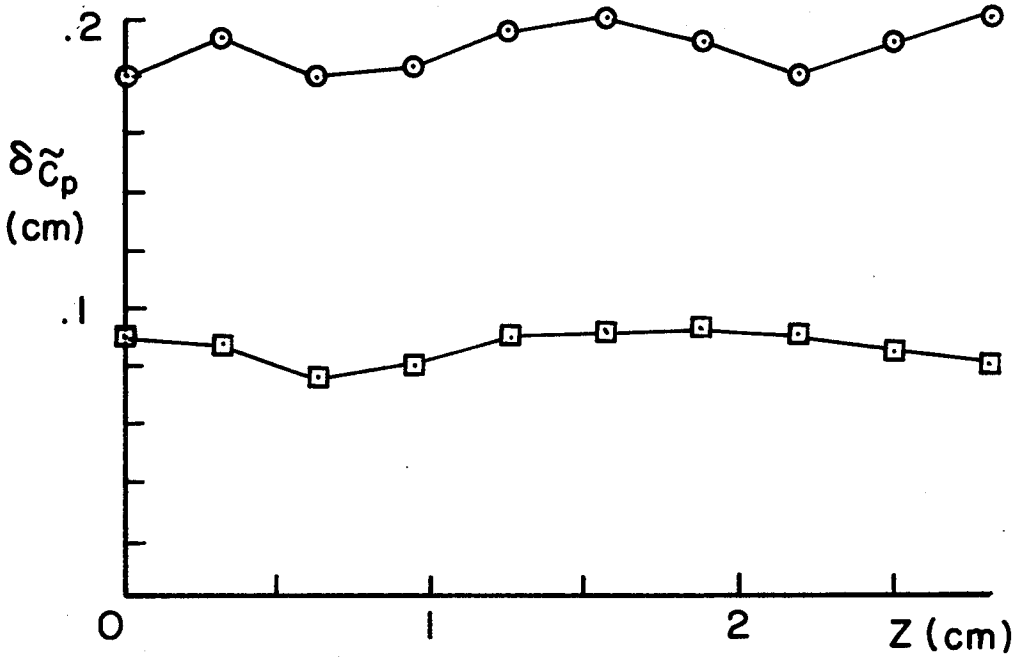

Figure II.11 Spanwise variation of product thickness. ⊡ , x = 4 cm, ⊙ , x = 9 cm.

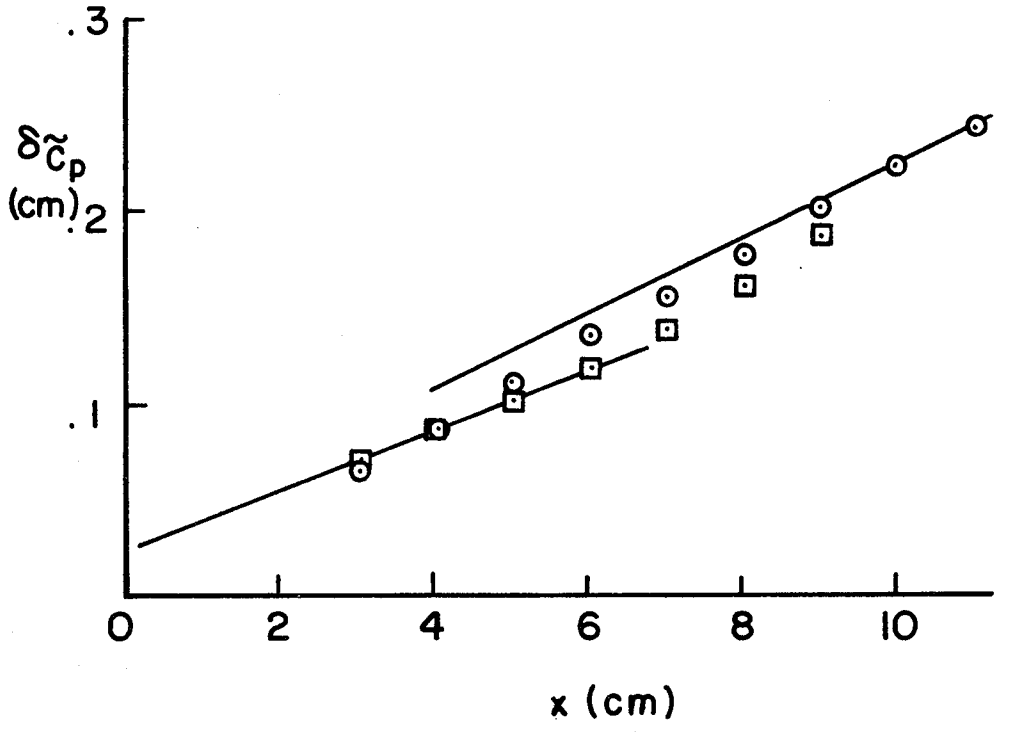

Figure II.12 Downstream growth of the product thickness at two spanwise locations: ⊙ , z = 0; ⊡ , z = 0.64 cm; (——), Konrad (1976).

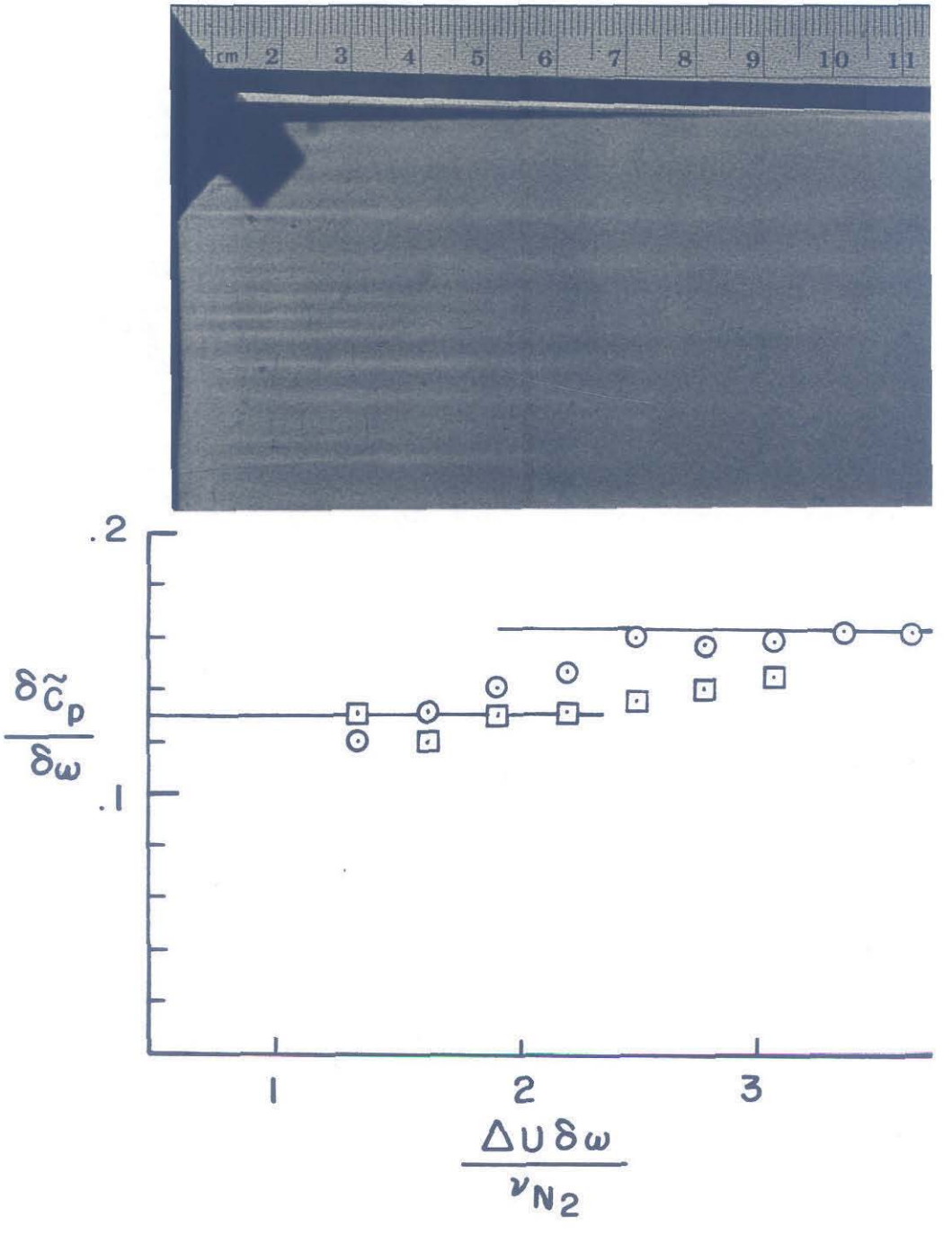

Figure II.13 Comparison between time exposure shadowgraph and product thickness growth rate at two spanwise locations: ⊙ , z = 0; ⊡ , z = 0.64 cm; (——), Konrad (1976).

(a)

(b)

Figure II.14 Cross-section pictures of the mixing layer in water. $Re_{\delta_\omega} \doteq 3 \times 10^3$.

(a) Cross-section through the core.
(b) Cross-section through the braid.

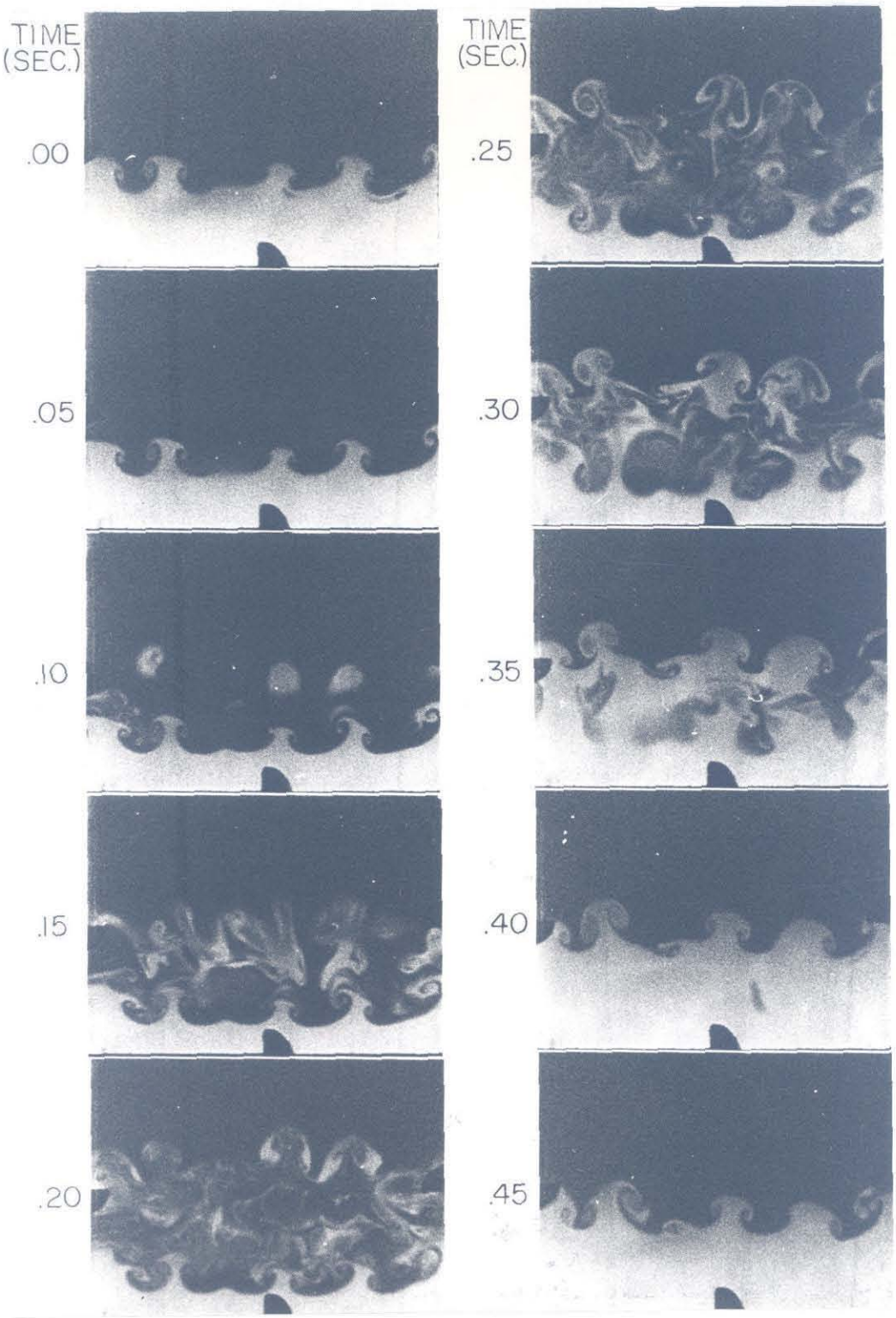

Figure II.15 Cross-section movie sequence of a primary vortex at $Re_{\delta_\omega} = 2.4 \times 10^3$.

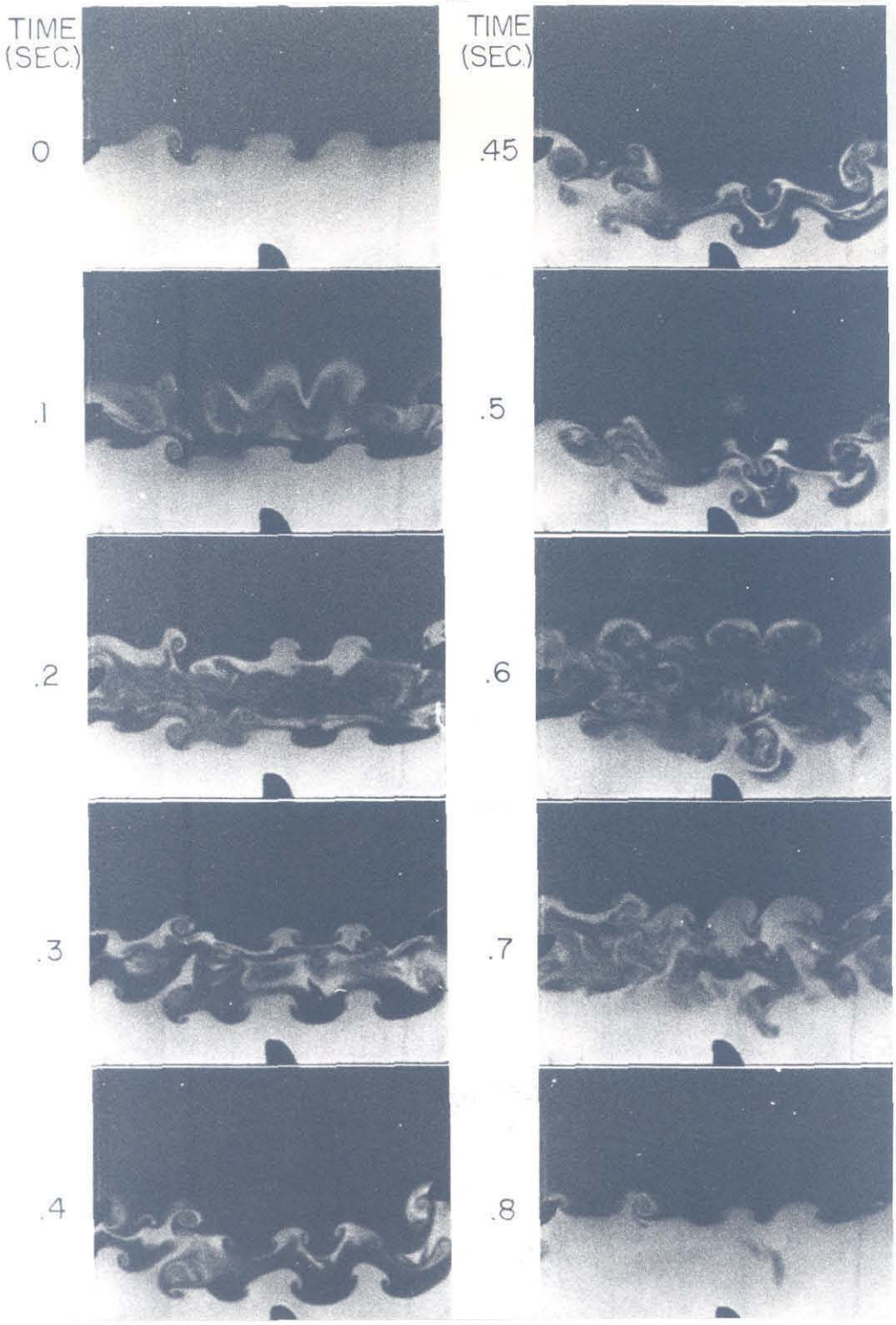

Figure II.16 Cross-section movie sequence of a primary vortex amalgamation $Re_{\delta_\omega} = 2.4 \times 10^3$.

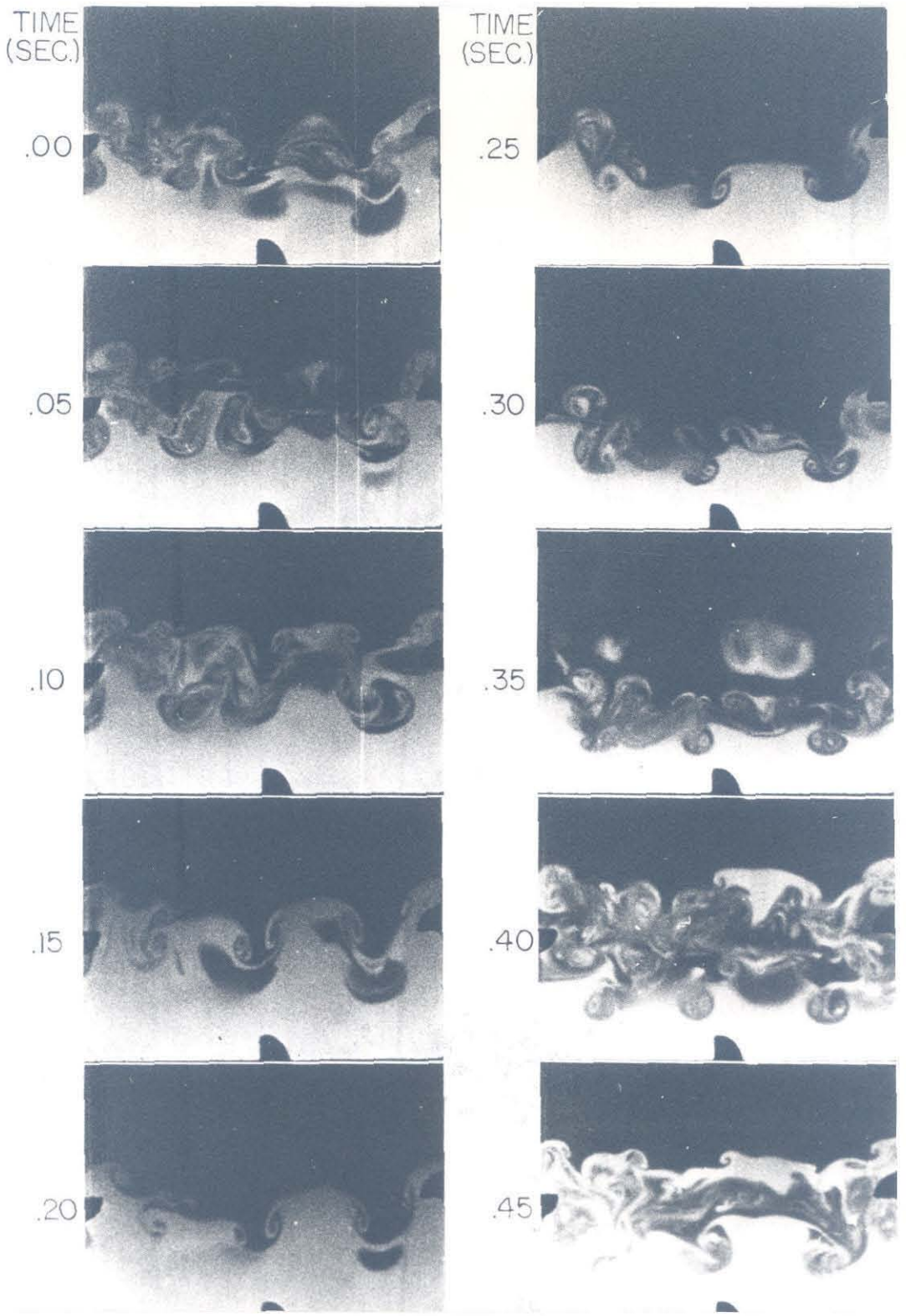

Figure II.17 Cross-section movie sequence of streamwise vortices $Re_{\delta_\omega} = 2.4 \times 10^3$.

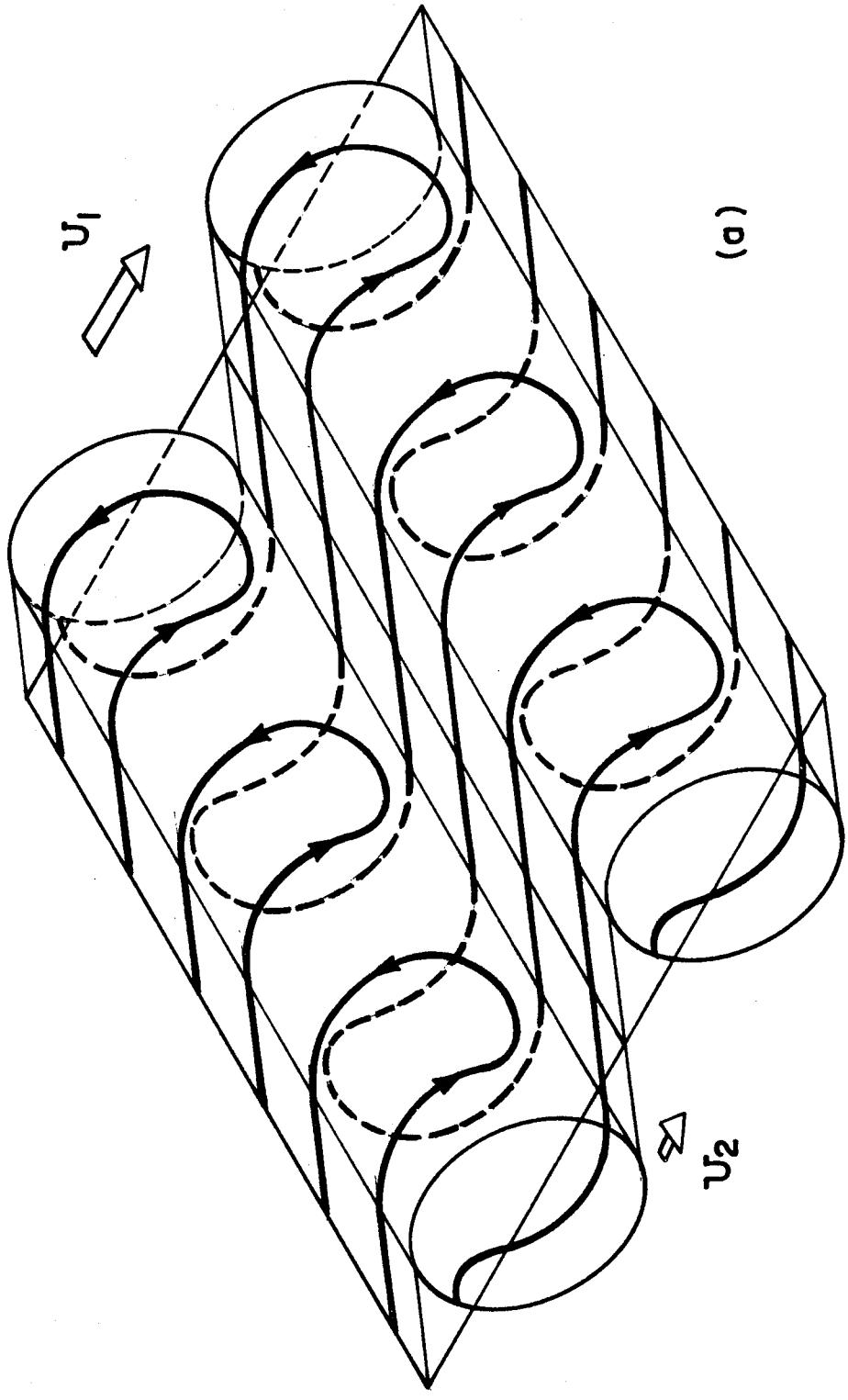

Figure II.18 Idealized picture of streamwise vortex structure.
(a) Isometric view
(b) Side view
(c) Plan view

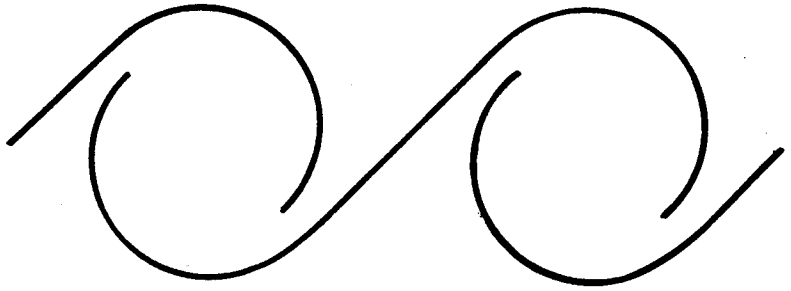

(b)

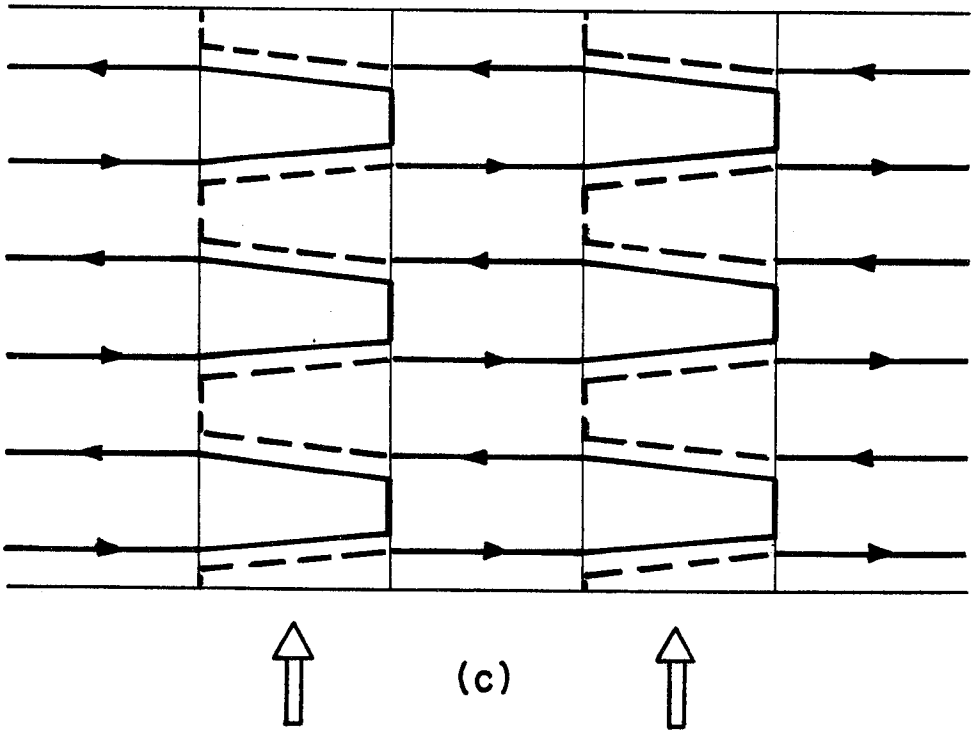

(c)

Figure II.18 See legend on page 91

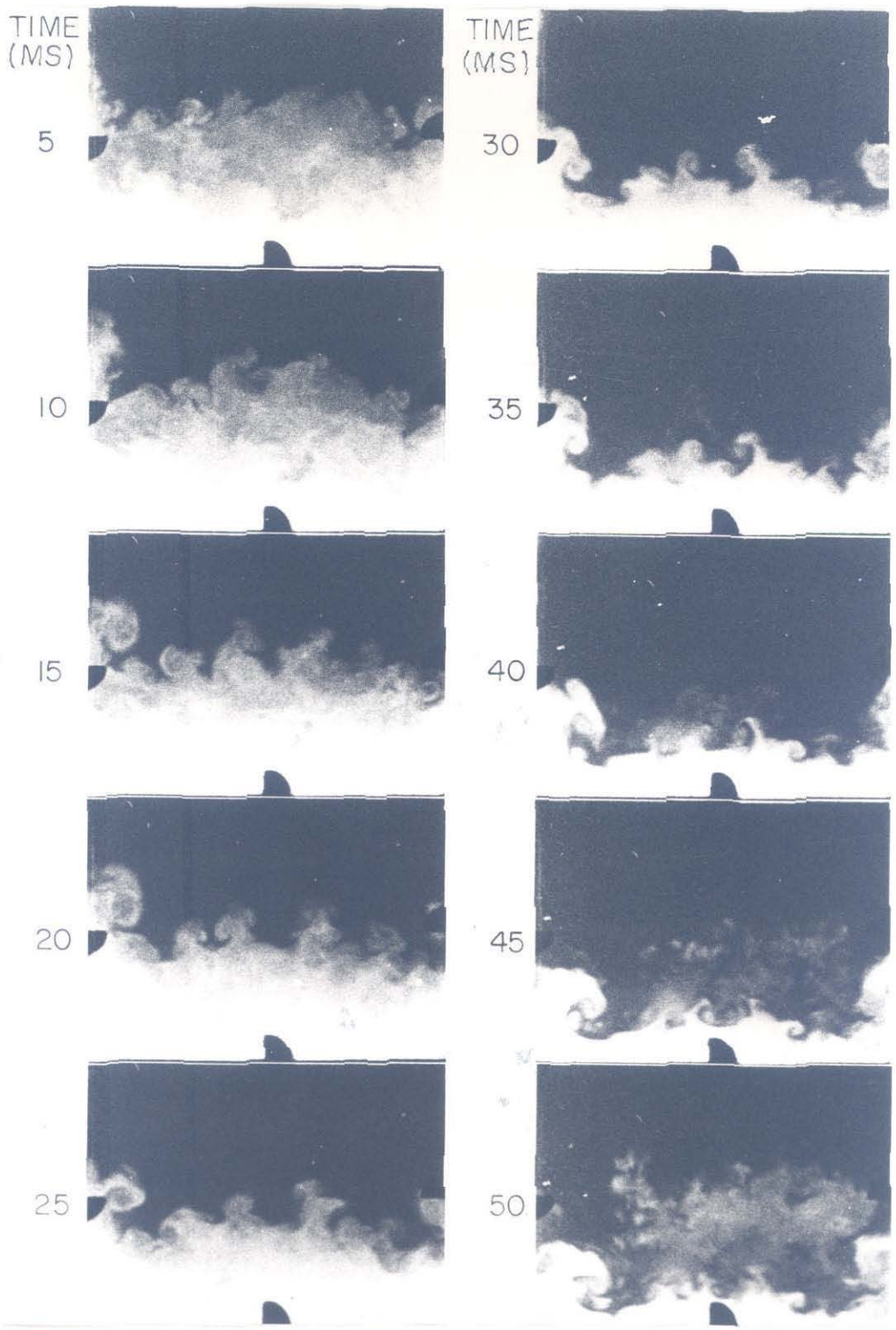

Figure II.19 Cross-section movie sequence of streamwise vortices along the braid. $Re_{\delta_\omega} = 10^4$.